Atmospheric and Fundamental Parameters of the Individual Components of Multiple Stellar Systems

Enas M. Abu-Alrob[1] , Abdallah M. Hussein[1] , and Mashhoor A. Al-Wardat[2,3,1]

[1] Department of Physics, Faculty of Sciences, Al al-Bayt University, PO Box 130040, Mafraq, 25113, Jordan; enas_aburub@yahoo.com
[2] Department of Applied Physics and Astronomy, College of Sciences, University of Sharjah, PO Box 27272 Sharjah, United Arab Emirates
[3] Sharjah Academy for Astronomy, Space Sciences and Technology, University of Sharjah, P.O. Box 27272 Sharjah, United Arab Emirates

Abstract

We present detailed analyses of eight triple stellar systems (lying between 20 and 155 pc) and nine quadruple stellar systems (lying between 20 and 250 pc) with different configurations. Most of these systems are hierarchical. The systems are HIP 4239, HIP 5588, HIP 11072, HIP 12548, HIP 13498, HIP 17895, HIP 19915, HIP 22607, HIP 25240, HIP 28614, HIP 41171, HIP 51255, HIP 51966, HIP 54611, HIP 78977, HIP 89234, and HIP 111805. We followed a method that can be applied to all multiple stellar systems, including the main sequence and subgiant evolutionary stages, to obtain their masses, ages, and atmospheric and fundamental parameters. These parameters were assured by the combined analysis of the astrometric measurements, photometric measurements, dynamical analysis, synthetic photometry, metallicity, and positions of the components on the H-R diagram. The estimated individual masses are of higher accuracy than those given by the dynamical solutions and listed in the MSC. The results show that all components of each of these systems have precisely the same age and metallicity. This ensures that fragmentation is the most probable theory for the formation of these multiple stellar systems. A quadratic fit was calculated for the mass–luminosity relation of the main-sequence subset components. We found that the primary component in all of these systems has evolved off the main-sequence stage, and some of these stars have already entered the subgiant stage.

1. Introduction

The study of binary and multiple stellar systems (BMSSs) has long been crucial to our understanding of star formation and development and continues to be a crucial area of research. This is largely due to advancements in imaging technology, which allow for better resolution and clearer observations of BMSSs, as well as improvements in radial velocity (RV) and metallicity measurements using stellar spectra. These advances have resulted in a significant increase in the number of BMSSs that can be analyzed using multiple techniques over the past 20 yr (Horch et al. 2015; Tokovinin et al. 2021).

The determination of the structure of BMSSs and the detailed analyses of such systems, which lead to the fundamental parameters and masses, are effective and active research tools for understanding the origin, evolution, and dynamics of stellar populations, as well as the mechanisms of star formation (Tokovinin 2018c; Al-Wardat et al. 2021a). Most stars are born in groups; hence, the properties of the components of binary and higher-order systems are very relevant (Tokovinin 2021).

The life and death of stars are also affected by their companions in various ways. Close pairs can form within hierarchical and nonhierarchical systems by their dynamical evolution on a long (compared to the formation) timescale. Knowing the exact ages of stars has always been a challenge in astrophysics. What simplified the matter is the knowledge of the relationship between the star age and its mass

Mardini et al. (2019a, 2019b). Observational knowledge of multiplicity has evolved from rudimentary descriptions of small and complete samples of neighboring solar-type stars to a more detailed statistical assessment of diversity across mass ranges and different environments (Duquennoy & Mayor 1991; Raghavan et al. 2010; Duchêne & Kraus 2013). Extensive multiplicity surveys, which mainly focus on binary coefficients, have recently discovered a strong dependence of multiplicity on mass and found that statistics on large multiplicity depend on the density and temperature of the formation medium and its metallicity (Moe & Di Stefano 2017). The main aim of this study is to analyze a set of nearby hierarchies of multiple stellar systems, which consist of three or four stars, and determine if there is a relation between their structure, fundamental parameters, and metallicities and thus determine their formation process and ages. In order to do so, we first estimate the atmospheric and fundamental parameters of the individual components of the systems, which include effective temperatures, logarithms of surface gravity, radii, luminosities, luminosity classes, absolute magnitudes, spectral types, and masses. This was done using Al-Wardat's method for analyzing BMSSs, and the masses were compared with the total masses calculated using the orbital solutions available. Using the estimated parameters, we can plot the components of each system on the Hertzsprung–Russell (H-R) diagram, isochrones, and age line. From this, we can determine whether the components were formed from the same cloud at the same time or not and hence define the evolutionary stage of each system (Mardini et al. 2022b).

The sample was selected based on the structures for triple and quadruple systems and the availability of information and observations on primary and subsystems in different catalogs.
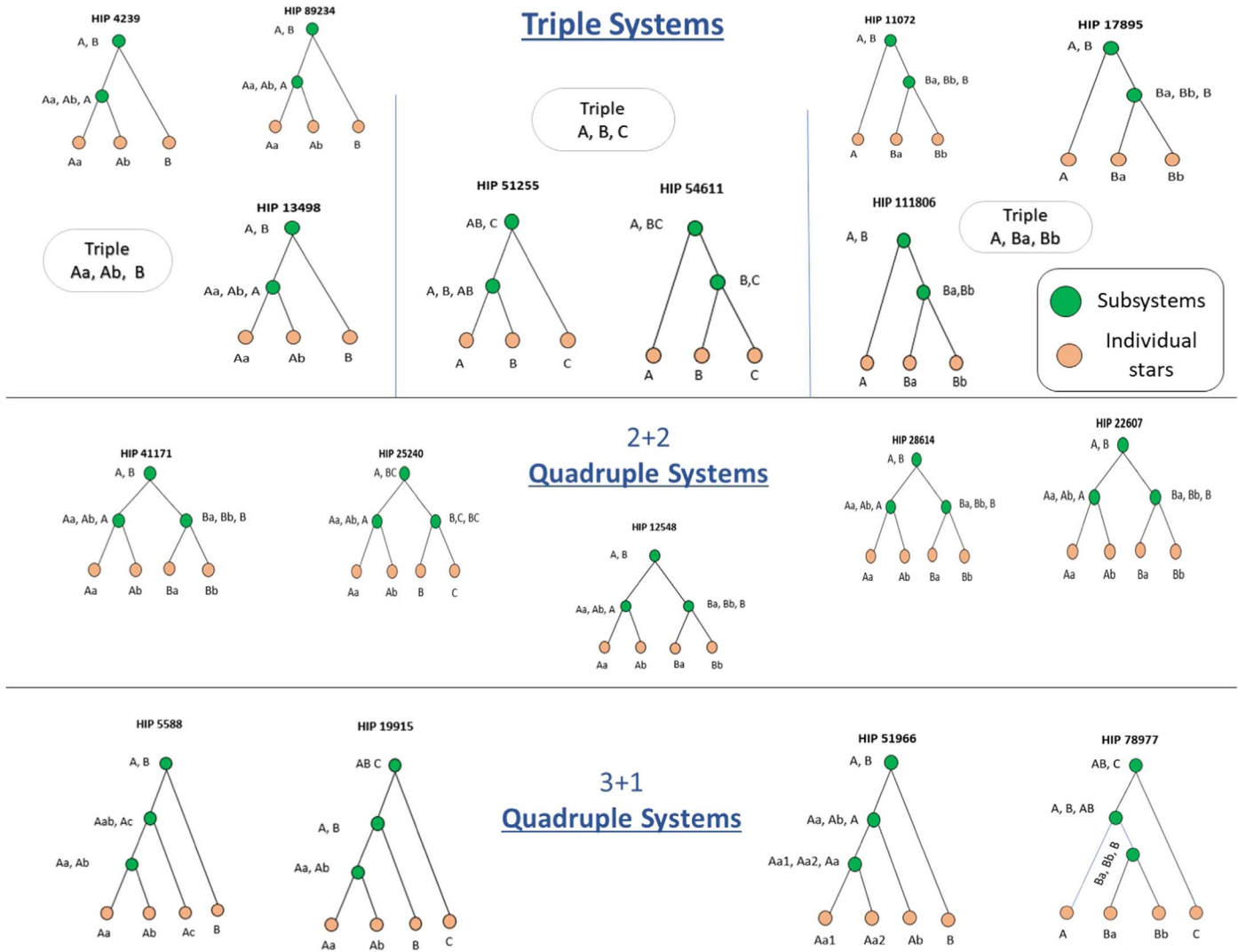
Figure 1. The structures of the 17 systems are analyzed here. Green circles denote subsystems designated as primary, secondary, or parent, while orange circles denote individual stars.

These systems are seen as a single star, even with giant telescopes, which means there is no way to observe the flux of any individual component.

The structures of our sample are shown in Figure 1. Among the sample, there are eight triple systems. Three of them (HIP 4239, HIP 13498, and HIP 89234) are triples with a subsystem in A as (Aa, Ab), three systems (HIP 11072, HIP 17895, and HIP 111805) are triples with a subsystem in B as (Ba, Bb), and two are ABC triple systems that are almost equilaterally triangular (HIP 51255 and HIP 54611). The rest of the samples are quadruple systems with two different hierarchical structures. The two-tier hierarchy (two close binaries orbiting each other) is also called a 2+2 quadruple, such as HIP 12548, HIP 22607, HIP 25240, HIP 28614, and HIP 41171. In the three-tier hierarchy, a close binary has a tertiary component, and this triple is orbited by another distant star, such as HIP 5588, HIP 19915, HIP 51966, and HIP 78977. These systems are called a 3+1 or "planetary" hierarchy.

Table 1 lists the primary archived data of the 17 systems. The columns are Hipparcos identifier, Washington Double Star Catalog (WDS) identifier, combined (entire) visual magnitude taken from ESA (1997), color index taken from (ESA 1997),

reduced Hipparcos trigonometric parallax taken from (Van Leeuwen 2007), Gaia DR2 trigonometric parallax taken from (Gaia Collaboration 2018), Gaia DR3 trigonometric parallax taken from (Gaia Collaboration et al. 2021), parallax zero-point correction of Gaia DR3 (Lindegren et al. 2021), iron abundance relative to the Sun [Fe/H], calculated metallicity Z, and number of components as given in the Multiple Star Catalog (MSC; Tokovinin 2018d). Multiple stellar systems can be dynamically stable hierarchical systems that can be decomposed into a combination of binaries.

Lindegren et al. (2021) provided an interim recipe that corrects the parallax of a given Gaia DR3 source for zero bias. This correction, which applies to Gaia DR3 astrometry, is in Python code gaiadr3zeropoint. The correction is provided using astrometric parameter solutions and given as a function of source magnitude, color, and celestial position. More details about the parallax zero-point correction are presented in (Mardini et al. 2022a, 2022b).

2. Method

The main issue of discovered BMSSs is that they appear as a single star even when being observed using large ground-based

Table 1
Object Identification and Observations

HIP WDS (1)	V_{Hip} (mag) (2)	$B-V$ $\pm$, (mag) (3)	B_T $\pm$, (mag) (4)	V_T $\pm$, (mag) (5)	π_H $\pm$, (mas) (6)	π_{G2} $\pm$, (mas) (7)	π_{G3} $\pm$, (mas) (8)	π_{G3}^{zp} $\pm$, (mas) (9)	[Fe/H] $\pm$, (dex) (10)	Z (11)	N_{Comp} (12)
4239 00541+6626	7.05	0.402 0.004	7.5 0.005	7.104 0.005	9.78 0.51	9.4876 0.0532	9.7544 0.0513	−0.02688	0.01 (1)	0.019	3
5588 01117+2243	7.57	0.338 0.015	7.974 0.009	7.591 0.009	3.36 0.60	4.3935 0.0677	4.6886 0.0315	−0.036853			4
11072 02225−2349	5.19	0.608 0.017	5.943 0.004	5.265 0.003	45.53 0.82	44.0905 0.2038	42.9117 0.4166	−0.023245	−0.10[2]	0.016	3
12548 02415−7128	7.76	0.700 0.002	8.658 0.011	7.857 0.009	18.60 0.81	15.8437 0.2038	… 0.02	…	0.12[2]	0.026	4
13498 02539−4436	7.70	0.648 0.010	8.489 0.009	7.786 0.008	14.09 0.73	6.7724 1.1456	11.9650 0.3677	−0.012069	0.13 (1)	0.027	3
17895 03496−0220	7.22	0.587 0.011	7.921 0.009	7.29 0.009	19.63 0.66	…	…	…	−0.09[1]	0.016	3
19915 04163+3644	8.96	0.642 0.015	9.602 0.023	9.049 0.022	4.94 1.2	6.0058 0.0719	6.0227 0.0202	−0.034122	−0.36[1] 0.10	0.0089	4
22607 04518+1339	6.30	0.502 0.007	6.857 0.006	6.314 0.005	24.56 1.00	22.6608 0.5253	22.6711 0.4122	−0.036602	0.15[1] 0.05	0.019 − 0.03	4
25240 05239−0052	6.13	0.483 0.009	6.695 0.006	6.143 0.006	17.95 0.77	19.2207 0.0816	19.5279 0.0868	−0.030141	0.12 (1)	0.026	4
28614 06024+0939	4.12	0.170 0.002	4.347 0.003	4.150 0.002	21.05 0.68	16.6954 1.4291	…	…	−0.07[1] 0.33	0.019	4
41171 08240−1548	8.57	0.442 0.099	9.139 0.018	8.685 0.013	5.72 1.28	6.6129 0.3235	4.9376 0.0309	−0.023782	−0.03	0.019	4
51255 10282−2548	8.51	0.672 0.096	9.179 0.017	8.532 0.015	11.22 1.16	9.4236 0.2089	11.0998 0.1679	−0.024685	−0.07[4]	0.017	3
51966 10370−0850	7.05	0.625 0.007	7.782 0.009	7.137 0.008	25.09 1.24	28.1461 0.4709	26.3036 0.4013	−0.032797	−0.20[1] 0.10	0.013	4
54611 11106−3234	7.24	0.456 0.010	7.779 0.008	7.294 0.007	6.80 0.60	6.4738 0.3684	7.4857 0.135	−0.024464	0.00[3]	0.020	3
78977 16073−2204	8.70	0.654 0.022	9.516 0.022	8.788 0.019	8.57 1.17	6.8719 0.0849	6.626 0.058	−0.034971	0.00[5]	0.02	4
89234 18126−7340	5.86	0.464 0.004	6.446 0.003	5.951 0.003	23.73 0.46	23.7740 0.0573	23.6778 0.0399	−0.015809	0.23[1]	0.035	3
111805 22388+4419	6.82	0.581 0.005	7.522 0.005	6.897 0.004	26.18 0.60	…	…	…	−0.24[1] 0.10	0.012	3

References. (1) (Gáspár et al. 2016), (2) (Netopil 2017), (3) (Beers et al. 2017), (4) (Casagrande et al. 2011), (5) (Bochanski et al. 2018).

telescopes (e.g., Hilditch 2001). This type of stellar system can only be identified as a binary or multiple system using high-resolution observational techniques such as speckle interferometry (e.g., Labeyrie 1970; Balega & Tikhonov 1977) or by modern techniques like adaptive optics. High-resolution imaging observations can barely show that the system is a binary, triple, quadruple, or higher hierarchical composition, while high-resolution spectroscopy gives the RV of the subcomponent(s) only if the system has enough tilted rotational orbit.

The accurate orbital solutions of binary and multiple stellar systems need several accurate positional measurements that are distributed well on the orbital period, which is not available for most of BMSSs. So an orbit needs to be based on a much larger number of observations. The more computation is based on well-determined quantities, the better the chances are of practical success. Hence, we need a different method for analyzing the multiple systems based on well-determined quantities.

One of these computational methods is Al-Wardat's method for analyzing BMSSs (Al-Wardat et al. 2021a). The method was first introduced in 2002 (Al-Wardat 2002). Since then, it has been used for the estimation of the atmospheric and fundamental parameters of the components of BMSSs. It was successfully and accurately used to analyze several systems (see, e.g., Al-Wardat 2009, 2009, 2012; Al-Wardat et al. 2014a, 2014b, 2021b;Masda et al. 2019; Al-Tawalbeh et al. 2021; Yousef et al. 2021; Hussein et al. 2022) and for analyzing multiple hierarchical systems like

the quadruple system ADS 11061 (Al-Wardat 2002; Masda et al. 2019). Moreover, it helps explain the formation process of BMSSs using their estimated metallicities and ages. The method can be applied to all types of binaries, visual, spectroscopic, and eclipsing, that have not evolved to a giant stage. The method was also used as an effective tool to verify the accuracy of the measured trigonometric parallaxes given by Hipparcos and Gaia astrometric missions and to estimate a new dynamical parallax once the orbit of the system is accurately solved (say, grade 1 or 2; Al-Wardat et al. 2021a, 2022; Tanineah et al. 2022).

The method employs Kurucz line-blanketed plane-parallel model atmospheres for each subcomponent depending on some preliminary calculations and available observational data like apparent visual magnitude, color index, and magnitude difference between each component. It uses these to build synthetic individual spectral energy distributions (SEDs), then builds the synthetic SED for the composed system using the following relation Al-Wardat (2002, 2012):

$$F_\lambda \cdot d^2 = \sum_{i=1}^{n} H_\lambda^i \cdot R_i^2, \qquad (1)$$

where F_λ is the synthetic flux density for the composed system (entire), d is the distance to the system in parsecs, n is 3 (triple system) or 4 (quadruple system), R_i is the radius of the component in solar units $R_\odot$, and H_λ^i are the synthetic fluxes of the component, which can be taken from any suitable model atmosphere. In this study, we adopted grids of plane-parallel line-blanketed model atmospheres of single stars, computed using the robust open-source program ATLAS 9 (Kurucz 1993, 1995; Castelli & Kurucz 2003), to build synthetic SEDs for the individual components, starting with calculated effective temperatures, logarithms of surface gravity, and radii based on the observations (visual magnitude, color index $(B - V)$, and visual magnitude difference).

The input values for model atmospheres are calculated from the observations (like magnitudes, magnitude differences, and color indices). Magnitude differences were taken from the MSC when available, and if not, we used the individual masses with the following relation (Docobo & Andrade 2013):

$$\triangle m = -\frac{5}{2} k \log\left(\frac{\mathcal{M}_2}{\mathcal{M}_1}\right), \qquad (2)$$

where $\mathcal{M}$ is the mass of the star component in $\mathcal{M}_\odot$, and k is a constant equal to 4.23 for main-sequence stars and 3.64 for subgiant stars.

Then, synthetic photometry is utilized to calculate the magnitudes and color indices of the synthetic SEDs. The synthetic magnitudes and color indices of the individual synthetic SEDs and the entire systems are calculated by integrating the absolute fluxes over each bandpass of a particular photometric system divided by that of the reference star (Vega) using the following equation (Al-Wardat 2012):

$$m_p[F_{\lambda,s}(\lambda)] = -2.5 \log \frac{\int P_p(\lambda) F_{\lambda,s}(\lambda) \lambda d\lambda}{\int P_p(\lambda) F_{\lambda,r}(\lambda) \lambda d\lambda} + ZP_p \qquad (3)$$

where m_p is the synthetic magnitude of the passband p, $P_p(\lambda)$ is the dimensionless sensitivity function of the passband p, $F_{\lambda,s}(\lambda)$ is the synthetic SED of the object, and $F_{\lambda,r}(\lambda)$ is the

SED of the reference star (Vega). Zero-points (ZP_p) from Maíz Apellániz (2007) are used.

The passbands of the three photometric systems employed in the synthetic photometry of Al-Wardat's method are Johnson U, B, V, and R; Strömgren u, v, b, and y; and Tycho B_T and V_T.

Once we get the best fit between the synthetic and observational parameters (magnitudes, magnitude differences, and color indices of the entire system), we can proceed with calculating the rest parameters using the following standard astrophysical equations:

$$\log \frac{L}{L_\odot} = 2 \log \frac{R}{R_\odot} + 4 \log \frac{T_{\text{eff}}}{T_{\text{eff}}^\odot}, \qquad (4)$$

$$M_{\text{bol}}^\odot - M_{\text{bol}} = 2.5 \log \frac{L}{L_\odot}. \qquad (5)$$

The errors of the values of the luminosities are calculated in this analysis depending on the following equation:

$$\sigma_L \approx \pm 2L \sqrt{\left(\frac{\sigma_R}{R}\right)^2 + 4\left(\frac{\sigma_{T_{\text{eff}}}}{T_{\text{eff}}}\right)^2}, \qquad (6)$$

where the errors of the stellar effective temperatures and radii of the individual components are estimated analytically by the method

$$M_V = M_{\text{bol}} - \text{BC}, \qquad (7)$$

where $T_\odot = 5777$ K, $R_\odot = 6.69*10^8$ m, and $M_{\text{bol}}^\odot = 4.75$ mag. Bolometric correction (BC) and spectral types are taken from the last version of Pecaut & Mamajek (2013) in (2022.04.16).

When the effective temperature, T_{eff}, and radii, R, for each star component are determined, the positions of these components on the H-R diagram can be established. This, in turn, enables estimation of their masses and ages through the use of evolutionary tracks and isochrones, such as those provided by Girardi et al. (2000a, 2000b), as it fulfills the required purpose for different metallicities, from which we can estimate the masses and ages of the individual components of the system.

Girardi et al. (2000a, 2000b) presented large grids of stellar evolutionary tracks, which are suitable for modeling star clusters and galaxies through population synthesis. They are presented as tracks for the initial chemical compositions $[Z = 0.0004, Y = 0.23]$, $[Z = 0.001, Y = 0.23]$, $[Z = 0.004, Y = 0.24]$, $[Z = 0.008, Y = 0.25]$, $[Z = 0.019, Y = 0.273]$ (solar composition), and $[Z = 0.03, Y = 0.30]$. The range of initial masses goes from 0.15 to 7 $\mathcal{M}_\odot$, and the evolutionary phases extend from the zero-age main sequence until either the thermally pulsing asymptotic giant branch regime or carbon ignition.

The metallicity Z can be calculated using measurements of iron abundance [Fe/H] (compared to that of the Sun) using the following relation (Bertelli et al. 1994):

$$Z^* = Z_\odot 10^{[\text{Fe/H}]}, \qquad (8)$$

where $Z_\odot = 0196 \pm 0.0014$ (Von Steiger & Zurbuchen 2016; Vagnozzi 2019).

As we mentioned in the Introduction, mass represents the core parameter of stellar astrophysics. That is why we are giving it special attention here. We have two ways to figure out masses: the estimation using Al-Wardat's method, depending on the positions of the components on the H-R diagram, and

the mass sum, which can be calculated using orbital parameters along with Kepler's third law.

The two methods are used in a diverging iterated process to get the precise masses of the individual components of the systems. The conclusion of Al-Wardat et al. (2021a, 2022) that the discrepancy in the parallax does not significantly affect the estimated masses using Al-Wardat's method, while it does have a clear impact on the dynamical mass sum, means that we can use the estimated masses to calculate a dynamical parallax for the system. This parallax can be used to calculate the dynamical mass sum and so on until we get the best fit between the estimated masses of Al-Wardat's method and the dynamical mass sum. Of course, we first use the available orbital parameters along with the trigonometric parallax measurements of Hipparcos 2 (Van Leeuwen 2007), Gaia DR2 (Gaia Collaboration 2018), and Gaia DR3 to calculate different options for the dynamical mass sum.

3. Analysis of Triple Systems

In this study, we analyze eight triple stellar systems. Three of them (HIP 4239, HIP 13498, and HIP 89234) are hierarchical triples structures with a subsystem in A as (Aa, Ab), three systems (HIP 11072, HIP 17895, and HIP 111805) are hierarchical triples structures with a subsystem in B as (Ba, Bb), and two are nonhierarchical ABC triple systems (HIP 51255 and HIP 54611).

Figure 2 shows the best fit for the composed synthetic SED for eight triple systems (black lines). The dotted and dashed lines are the synthetic SEDs for the individual stars. Moreover, the Johnson magnitude system from Table 1 can be converted to flux density F_λ in units of erg cm^{-2} s^{-1} Å^{-1}, where the effective central wavelength for the blue filter is 4353 nm and that for the visual filter is 5477 nm. The blue points are the measured blue magnitude by the Johnson filter and the green points are the measured visual magnitude by the Johnson filter (from Hipparcos ESA 1997).

Table 2(a) lists the 17 parameters obtained in the present work for the triple stellar systems. Systems HIP 4239, HIP 11072, HIP 13498, HIP 17595, HIP 89234, and HIP 111805 are hierarchies, while the other two are equilateral triangle configurations.

Table 2(b) lists the atmospheric and fundamental parameters of the eight triple systems as obtained in the present work. The columns give the Hipparcos identifier, effective temperatures $T_{\rm eff}$, radii R, logarithm of gravity acceleration $\log g$, luminosities L, bolometric magnitudes $M_{\rm bol}$, absolute visual magnitudes M_V, individual mass $\mathcal{M}$, spectral types Sp, and ages. Masses and ages are estimated from the positions of the subcomponents on the H-R diagram, evolutionary tracks, and isochrones, which are taken from Girardi et al. (2000a).

3.1. HIP 4239

The triple system YSC 19 (HD 5110) consists of a subsystem (Aa, Ab). The orbit of the subsystem (Aa, Ab) was first solved independently using both positional measurements and the CfA RVs, which cover a period of 16 yr. The outer physical component B is located 0″9 from the primary subsystem and has been moving slowly for approximately 500 yr. The orbit of the primary system (A, B) is not solved yet.

In this work, we use a magnitude difference of the primary system (AB) of $\triangle m_V^{\rm AB} = 3.81$ mag and the subsystem (Aa, Ab)

of $\triangle m_V^{\rm Aa,Ab} = 0.6$ mag. Both values were taken from MSC (Tokovinin 2018c). We estimate the atmospheric parameters and calculate the system component fundamental parameters using Al-Wardat's method. The method uses these parameters to build synthetic SEDs and give the positions of the system's components on the H-R diagram, the evolutionary tracks, and the isochrones of Girardi et al. (2000b; see Figure 3). Our analysis shows that the three components are of solar metallicity with an age of 1.413 Gyr with evolved components (Aa and Ab) and a dwarf main-sequence component (B).

Tokovinin (2019a) suggested that Ab could be a subsystem depending on some detectable spectroscopic features in the lines of the component. However, their RVs do not match the expected RVs in the 11 yr orbit. The estimated mass sum using Al-Wardat's method is $\Sigma\mathcal{M} = 4.01\ \mathcal{M}_\odot$, which is consistent with the mass sum obtained in earlier studies from the MSC (Tokovinin 2018c; see Table 2). The estimated mass sum of subsystem Aa, Ab is $\Sigma\mathcal{M}_{\rm H2} = 3.09\ \mathcal{M}_\odot$ using this result. A new dynamical parallax of $\pi_{\rm dyn} = 10.0635 \pm 0.37$ mas is calculated for the system using Equation (9).

3.2. HIP 11072

The bright nearby solar-type dwarf triple system HD 14802 (κ For) consists of a subsystem (Ba, Bb) of M-type dwarfs with a tentative period of 3.7 days orbiting the main component (A) with an orbital period of 26 yr (Tokovinin 2013). The system is known as a spectroscopic binary. In 1993 January, Güdel et al. (1995) detected microwave radiation from a nearby solar-type dwarf located 0″23 south of the star κ For. They suggested that the radio emission came from a secondary tight M dwarf pair (Ba, Bb), and its mass sum is similar to the mass of A. Hence, the emissions cause diffraction in the photocenter. The astrometric and spectroscopic companion was first resolved in 2005 by Lafreniere et al. (2007). Later, in 2007, Tokovinin & Cantarutti (2008) and Hartkopf et al. (2012) independently calculated the first visual orbit using all resolved measurements; the orbit is classified as grade 4. Tokovinin (2013) derived the combined interferometric/spectroscopic orbit, which corresponds to the astrometric orbit.

Nielsen & Close (2010) estimated the age of the system as 4 Gyr for the primary component and 6.3 Gyr for the secondary component, citing these estimates from the lithium line strength and rotation. Despite the age of this system, its high activity and the rapid axial rotation of the M dwarfs are maintained by synchronization with the orbit (Tokovinin 2013). Component A is located above the main sequence in the color–magnitude diagram ($V, B - V$), which means that it is an evolved star at the beginning of the subgiant phase.

In this work, we used the magnitude difference for the primary system (AB) as $\triangle m_V^{\rm AB} = 4.91$ mag and the subsystem (Ba, Bb) as $\triangle m_V^{Ba,Bb} = 0$ mag as given in MSC. The results of the atmospheric parameters and calculated fundamental parameters are listed in Table 2. Figure 4 shows the positions of the system's components on the H-R diagram with the evolutionary tracks and age line of 3.981 Gyr. We can see that component A has already left the main sequence to the subgiant phase, while the other two components (Ba, Bb) are still in the main-sequence phase. This result agrees with the results of Nielsen & Close (2010). The calculated individual masses and mass sum are listed in Table 2. For HIP 11072, the calculated mass sum in this work is close to the mass sum given in MSC.
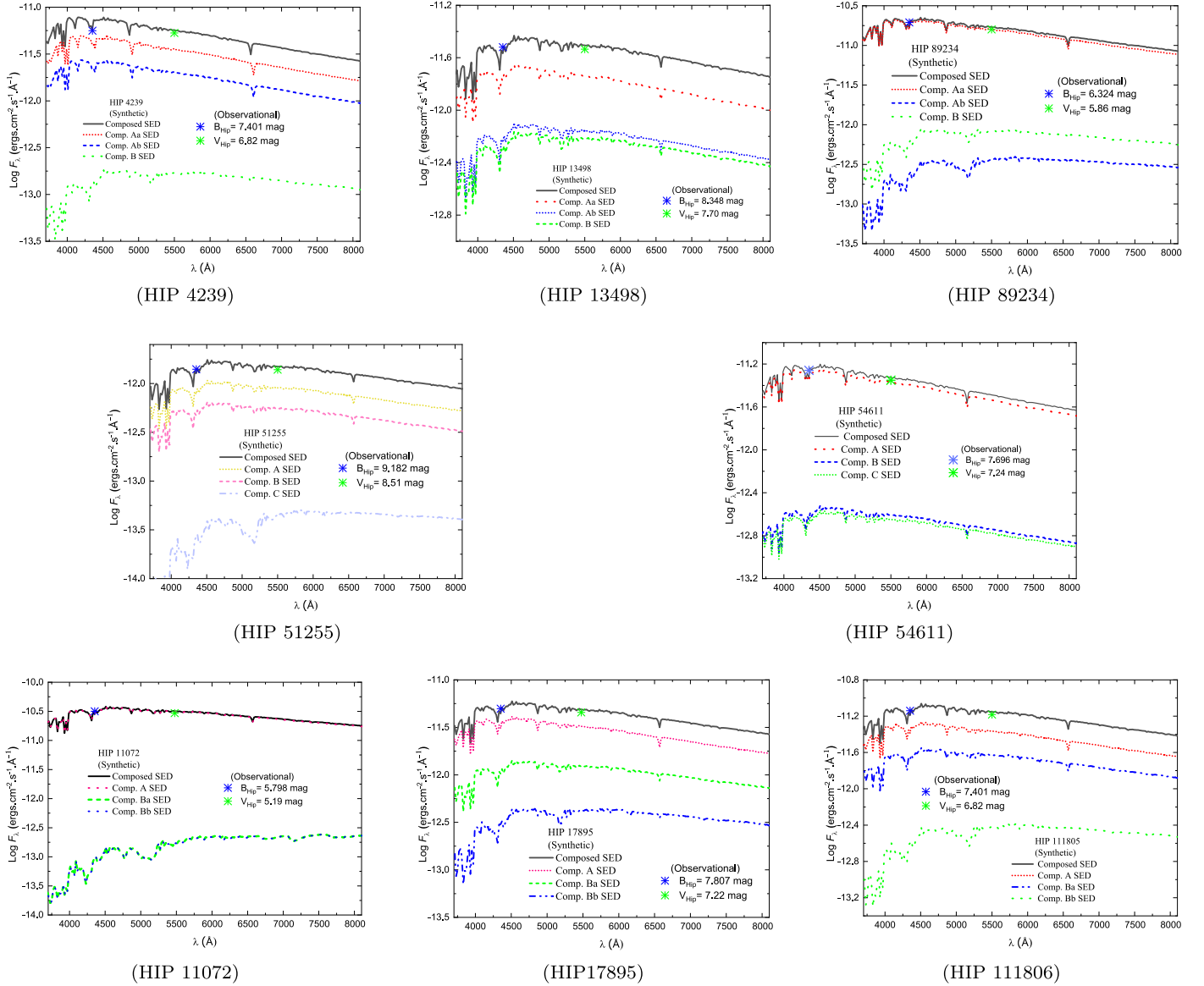
Figure 2. Synthetic SED diagrams for the eight triple systems. The three dotted and dashed lines are the synthetic SEDs from the individual stars, while the black line is the sum of the individual SEDs (composed). The blue points are the calculated flux density using the measured blue Johnson magnitude, and the green points are the calculated flux density using the measured visual Johnson magnitude (from Hipparcos ESA 1997).

Fekel et al.'s (2018) orbital parameters, along with the calculated mass sum, are used to calculate a new dynamical parallax of $\pi_{dyn} = 44.55 \pm 0.50$ mas. This value lies between the Hipparcos 2 and Gaia DR2 parallaxes.

3.3. HIP 13498

The spectral type of the system HD 18198 is given in SIMBAD as G8/K1III+(F) (Houk 1978). But in fact, we found that all of its components are main-sequence dwarf stars. Wichmann et al. (2003) concluded that there is a spectroscopic subsystem depending on the detection of double lines. Ignoring the multiplicity, Casagrande et al. (2011) derived some of the physical parameters from high-resolution spectra as T_{eff} = 5925 K, [Fe/H] = 0.14, and $\log g$ = 4.03. Tokovinin (2016) derived the orbital elements of the visual orbit (A, B) and the orbital elements of the spectroscopic orbit of the subsystem (Aa, Ab). In addition, he calculated the mass sum of the system as $3.03 \mathcal{M}_\odot$, distributed as $\mathcal{M}_A = 2.16 \pm 0.40$,

$\mathcal{M}_B = 0.87 \pm 0.25 \mathcal{M}_\odot$. From the orbital solution of the main system and the mass sum, Tokovinin (2022) calculated a dynamical parallax of $\pi_{dyn} = 14.8 \pm 0.8$ mas.

Tokovinin (2016) derived effective temperatures, color indices, absolute magnitudes, and individual masses from the Gaussian fits of the lithium lines as follows: component Aa ($T_{eff}^{Aa} = 6103$ K, $B - V = 0.51$ mag, $M_V^{Aa} = 4.17$ mag, and $\mathcal{M}_{Aa} = 1.11 \mathcal{M}_\odot$), component Ab ($T_{eff}^{Ab} = 5558$ K, $B - V = 0.78$ mag, $M_V^{Ab} = 5.22$ mag, and $\mathcal{M}_{Ab} = 0.96 \mathcal{M}_\odot$), and component B ($T_{eff}^B = 5443$ K, $B - V = 0.82$ mag, $M_V^B = 5.38$ mag, and $\mathcal{M}_B = 0.93 \mathcal{M}_\odot$). Later (Tokovinin 2018c), he gave the apparent magnitudes and individual masses of the components as follows: component Aa ($m_V^{Aa} = 8.31$ mag and $\mathcal{M}_{Aa} = 1.11 \mathcal{M}_\odot$), component Ab ($m_V^{Ab} = 9.36$ mag and $\mathcal{M}_{Ab} = 0.96 \mathcal{M}_\odot$), and component B ($m_V^B = 9.52$ mag and $\mathcal{M}_B = 0.93 \mathcal{M}_\odot$). This gives a mass sum for the whole system of $\Sigma \mathcal{M} = 3 \mathcal{M}_\odot$.

In this work, we used a magnitude difference for the main system (AB) of $\triangle m_V^{Ab} = 1.55$ mag and the subsystem (Aa, Ab)

Abu-Alrob, Hussein, & Al-Wardat

Table 2
(a) 17 Parameters for the Eight Triple Stellar Systems

Filter	Johnson							Strömgren							Tycho		
	U	B	V	R	$U-B$	$B-V$	$V-R$	u	v	b	y	$u-v$	$u-b$	$b-y$	B_T	V_T	B_T-V_T
HIP 4239																	
Obs.	⋯	7.452	7.05	⋯	0.02	0.402	⋯	⋯	⋯	⋯	⋯	⋯	⋯	0.248	7.50	7.104	0.396
Comp.	7.46	7.45	7.05	6.82	0.01	0.402	0.23	8.66	7.71	7.28	7.02	0.95	0.43	0.26	7.54	7.09	0.44
Aa	7.95	7.95	7.58	7.35	0.001	0.384	0.22	9.16	8.21	7.79	7.54	0.95	0.42	0.25	8.040	7.62	0.42
Ab	8.59	8.59	8.18	7.95	0.002	0.407	0.23	9.79	8.86	8.42	8.16	0.94	0.43	0.26	8.69	8.24	0.45
B	12.18	11.73	10.89	10.44	0.45	0.837	0.45	13.33	12.19	11.33	10.85	1.14	0.85	0.49	11.95	10.98	0.97
HIP 11072																	
Obs.	⋯	5.798	5.19	4.66	⋯	0.608	⋯	⋯	⋯	⋯	⋯	⋯	⋯	0.387	5.943	5.265	0.678
Comp.	5.91	5.79	5.19	4.85	0.11	0.609	0.34	7.07	6.123	5.53	5.16	0.94	0.59	0.37	5.95	5.26	0.69
A	5.91	5.80	5.20	4.87	0.11	0.60	0.33	7.07	6.13	5.54	5.17	0.93	0.59	0.37	5.95	5.27	0.68
Ba	13.38	12.20	10.86	10.04	1.18	1.34	0.82	14.83	12.95	11.65	10.81	1.88	1.29	0.84	12.51	11.05	1.47
Bb	13.39	12.21	10.86	10.05	1.18	1.34	0.82	14.84	12.95	11.66	10.82	1.88	1.29	0.84	12.52	11.05	1.47
HIP 13498																	
Obs.	⋯	8.348	7.70	⋯	⋯	0.648	⋯	⋯	⋯	⋯	⋯	⋯	⋯	0.391	8.489	7.786	0.703
Comp.	8.51	8.35	7.70	7.35	0.16	0.648	0.35	9.66	8.69	8.07	7.67	0.96	0.63	0.39	8.51	7.78	0.74
Aa	8.98	8.88	8.29	7.97	0.09	0.592	0.32	10.13	9.20	8.62	8.26	0.93	0.58	0.36	9.02	8.36	0.67
Ab	10.29	10.05	9.34	8.96	0.24	0.71	0.38	11.43	10.43	9.73	9.31	1.01	0.69	0.42	10.23	9.42	0.81
B	10.52	10.24	9.49	9.09	0.29	0.74	0.39	11.67	10.63	9.89	9.46	1.03	0.74	0.44	10.43	9.57	0.86
HIP 17895																	
Obs.	⋯	7.807	7.22	⋯	⋯	0.587	⋯	⋯	⋯	⋯	⋯	⋯	⋯	0.372	7.921	7.29	0.631
Comp.	7.91	7.81	7.22	6.90	0.10	0.587	0.32	9.07	8.13	7.55	7.19	0.4	0.58	0.36	7.95	7.29	0.66
A	8.22	8.18	7.66	7.37	0.04	0.52	0.29	9.39	8.48	7.96	7.64	0.91	0.52	0.32	8.30	7.72	0.58
Ba	9.64	9.43	8.72	8.37	0.21	0.69	0.37	10.78	9.79	9.12	8.71	0.99	0.67	0.41	9.60	8.82	0.79
Bb	11.38	10.83	9.90	9.47	0.54	0.88	0.48	12.54	11.33	10.41	9.90	1.21	0.91	0.51	11.07	10.04	1.03
HIP 51255																	
Obs.	⋯	9.182	8.51	⋯	⋯	0.672	⋯	⋯	⋯	⋯	⋯	⋯	⋯	0.377	9.179	8.532	0.647
Comp.	9.36	9.18	8.51	8.14	0.18	0.672	0.37	10.51	9.54	8.88	8.48	0.97	0.66	0.41	9.35	8.58	0.76
A	9.87	9.70	9.05	8.69	0.16	0.65	0.35	11.01	10.05	9.41	9.02	0.96	0.64	0.39	9.86	9.12	0.74
B	10.44	10.25	9.58	9.22	0.18	0.67	0.36	11.58	10.61	9.95	9.55	0.97	0.65	0.40	10.42	9.65	0.76
C	14.51	13.52	12.39	11.72	0.99	1.13	0.67	15.81	14.19	12.98	12.32	1.62	1.22	0.66	13.82	12.53	1.29
HIP 54611																	
Obs.	⋯	7.696	7.24	⋯	⋯	0.456	⋯	⋯	⋯	⋯	⋯	⋯	⋯	⋯	7.779	7.294	0.485
Comp.	7.71	7.69	7.24	6.99	0.02	0.455	0.26	8.90	7.98	7.51	7.22	0.94	0.47	0.29	7.80	7.29	0.50
A	7.81	7.79	7.36	7.11	0.01	0.44	0.25	8.99	8.07	7.61	7.33	0.93	0.46	0.28	7.89	7.41	0.49
B	11.24	11.15	10.57	10.25	0.09	0.59	0.32	12.39	11.47	10.89	10.54	0.93	0.58	0.36	11.29	10.63	0.66
C	11.37	11.27	10.67	10.34	0.11	0.60	0.33	12.53	11.59	11.01	10.64	0.93	0.59	0.37	11.41	10.73	0.68
HIP 89234																	
Obs.	⋯	6.324	5.86	⋯	0.03	0.464	⋯	⋯	⋯	⋯	⋯	⋯	⋯	0.302	6.446	5.951	0.495

Table 2
(Continued)

Filter	Johnson							Strömgren							Tycho		
	U	B	V	R	$U-B$	$B-V$	$V-R$	u	v	b	y	$u-v$	$u-b$	$b-y$	B_T	V_T	B_T-V_T
Comp.	6.34	6.32	5.86	5.59	0.02	0.464	0.26	7.53	6.60	6.13	5.83	0.93	0.48	0.29	6.43	5.91	0.51
Aa	6.38	6.37	5.93	5.68	0.01	0.44	0.25	7.57	6.64	6.19	5.91	0.93	0.45	0.28	6.47	5.99	0.48
Ab	11.91	11.11	10.10	9.51	0.79	1.01	0.58	13.14	11.71	10.62	10.03	1.43	1.09	0.58	11.39	10.22	1.17
B	10.55	10.04	9.18	8.71	0.50	0.86	0.47	11.71	10.52	9.63	9.14	1.18	0.89	0.49	10.28	9.27	1.01
HIP 111805																	
Obs.	⋯	7.401	6.82	⋯	⋯	0.581	⋯	⋯	⋯	⋯	⋯	⋯	⋯	0.376	7.522	6.897	0.625
Comp.	7.49	7.39	6.82	6.49	0.09	0.581	0.32	8.65	7.72	7.15	6.79	0.93	0.57	0.36	7.54	6.88	0.65
A	7.92	7.88	7.35	7.06	0.05	0.53	0.29	9.09	8.18	7.65	7.32	0.91	0.53	0.33	8.00	7.41	0.59
Ba	8.77	8.64	8.01	7.68	0.13	0.62	0.34	9.92	8.97	8.36	7.99	0.94	0.61	0.38	8.79	8.08	0.70
Bb	11.79	11.04	10.05	9.48	0.76	0.99	0.57	13.01	11.62	10.56	9.98	1.39	1.06	0.57	11.31	10.16	1.15

(b) Atmospheric and Fundamental Parameters of the Eight Triple Systems

Comp.	$T_{\rm eff}$, K	R, $R_\odot$	$\log g$, cm s^{-2}	L, $L_\odot$	$M_{\rm bol}$, mag	M_V, mag	$\mathcal{M}$, $\mathcal{M}_\odot$	Sp	Age,[a] Gyr
HIP 4239									
Aa	6870	2.26	3.93	10.21	2.23	2.25	1.63	F1.5/IV	1.413
Ab	6830	1.738	4.12	5.90	2.82	2.84	1.46	F2/IV	
B	5450	0.86	4.52	0.59	5.33	5.50	0.92	G8/V	
HIP 11072									
A	6060	1.928	3.96	4.5	3.12	3.20	1.25	F9/IV	3.981
Ba	4202	0.538	4.75	0.08	7.48	8.34	0.60	K6/V	
Bb	4200	0.5381	4.75	0.08	7.48	8.34	0.60	K6/V	
HIP 13498									
Aa	6107	1.48	4.19	2.74	3.66	3.73	1.25	F4/IV	2.818
Ab	5730	1.066	4.40	1.10	4.65	4.77	1.07	G3/V	
B	5670	1.028	4.42	0.98	4.77	4.90	1.04	G4/V	
HIP 17895									
A	6355	1.288	4.30	2.43	3.79	3.84	1.22	F6/V	1.778
Ba	5790	0.99	4.44	1.10	4.76	4.87	1.01	G2/V	
Bb	5190	0.78	4.60	0.40	5.75	6.01	0.85	K1/V	
HIP 51255									
A	5900	1.435	4.15	2.24	3.87	3.97	1.08	G0.5/IV	7.08
B	5845	1.15	4.31	1.39	4.40	4.41	1.01	G1.5/IV	
C	4610	0.676	4.62	0.19	6.58	7.13	0.71	K4/V	
HIP 54611									
A	6650	3.865	3.53	26.23	1.20	1.24	1.90	F4/IV	1.259
B	6120	1.12	4.39	1.58	4.25	4.32	1.14	F8/V	

Table 2
(Continued)

				(b) Atmospheric and Fundamental Parameters of the Eight Triple Systems					
C	6070	1.09	4.40	1.45	4.35	4.43	1.12	F9/V	
				HIP 89234					
Aa	6670	2.12	3.98	7.99	2.49	2.53	1.6	F4/IV	1.413
Ab	4850	0.743	4.59	0.27	6.15	6.56	0.8	K3/V	
B	5260	0.865	4.51	0.51	5.47	5.69	0.9	K0/V	
				HIP 111805					
A	6320	1.13	4.35	1.83	4.09	4.14	1.05	F6/V	3.548
Ba	6000	0.94	4.46	1.03	4.72	4.80	0.95	F9/V	
Bb	4900	0.665	4.64	0.23	6.35	6.70	0.71	K2.5/V	

Note.
[a] The isochrones are functions of the metallicity.
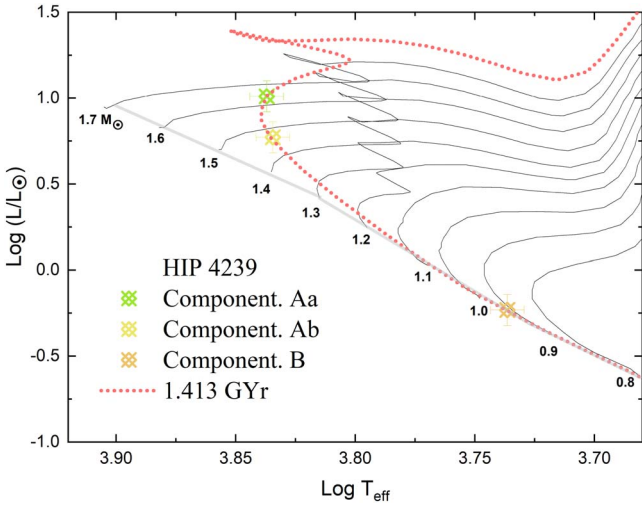
Figure 3. Analysis for HIP 4239. The positions of the components are shown on the H-R diagram with evolutionary tracks and the 1.413 Gyr isochrone with $Z = 0.019$.
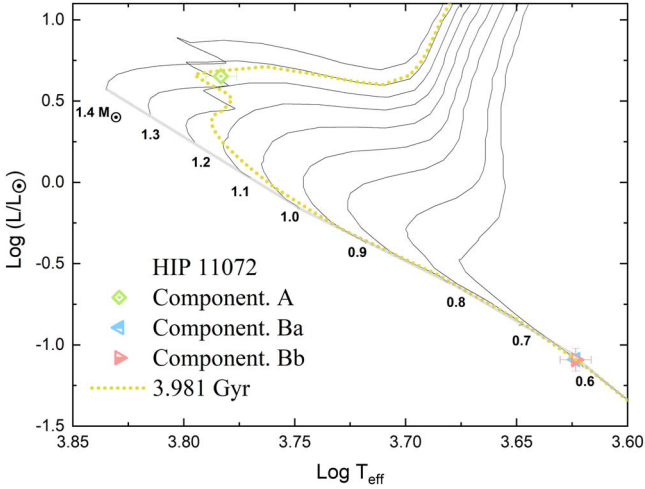

Figure 4. Analysis for HIP 11072. The positions of components are shown on the H-R diagram with evolutionary tracks and the 3.981 Gyr isochrone with $Z = 0.019$.

of $\triangle m_V^{AaAb} = 1.05$ mag. Both values were taken from MSC (Tokovinin 2018c). The results of the analysis as atmospheric and fundamental parameters are listed in Table 2. Figure 5 shows the positions of the system's components on the H-R diagram, the evolutionary tracks, and the age line of 2.818 Gyr. It shows that the component Aa evolved off the main sequence, while components Ab and B are still on the main sequence. If we compare masses, as listed in Table 4, we can see that there is an excellent consistency between the estimated mass sum in this work of $\Sigma \mathcal{M} = 3.36 \pm 0.11 \mathcal{M}_\odot$ with the dynamical one calculated using the orbital elements and the parallax of Hipparcos 2 of $\mathcal{M}_{dyn}^H = 3.48 \mathcal{M}_\odot$, while it disagrees with that calculated using Gaia DR2, $\mathcal{M}_{dyn} = 31.31 \mathcal{M}_\odot$. This shows the relative reliability of the Hipparcos measurements compared to Gaia DR2 and DR3, as noted by Al-Wardat et al. (2021a). Using the orbital parameters given by Tokovinin (2016) and estimated masses from Al-Wardat's method, we can estimate a new dynamical parallax for the system using Kepler's third law (Equation (9)) of $\pi_{dyn} = 14.25 \pm 0.5$ mas.

3.4. HIP 17895

This system is a nearby solar-type dwarf detected by the Geneva–Copenhagen Survey as a double-lined spectroscopic binary, and the mass ratio is $q = 0.577 \pm 0.109$; the same time, it was classified as a visual binary, YR 23. The primary system (A, B) was first resolved by (Horch et al. 2002) in 2000.76 at $0\overset{''}{.}28$. Such a system is usually solved by Hipparcos, but its duplicity has not been identified from that experiment. However, Hipparcos was able to identify the system as an astrometric binary but could not identify if it was a triple system. The orbit of this system has been updated (Gorynya & Tokovinin 2018) using the recent data and a fixed eccentricity of 0.6 because the orbit of this system is weak. The calculated mass is $\mathcal{M}_A = 1.14$, $\mathcal{M}_{Ba} = 0.96$, and $\mathcal{M}_{Bb} = 0.80 M_\odot$ or a mass sum of 2.9 $M_\odot$.

In this work, we used a magnitude difference for the primary system (AB) of $\triangle m_V^{AB} = 0.75$ mag and the subsystem (Ba, Bb) of $\triangle m_V^{BaBb} = 1.18$ mag, which were taken from MSC (Tokovinin 2018c). The results of the atmospheric parameters and calculated fundamental parameters are listed in Table 2(b).

Figure 6 shows the the positions of the system's components on the H-R diagram, the evolutionary tracks, and the age line of 1.778 Gyr. Component A starts to evolve off the main sequence, while components Ba and Bb are still on the main sequence.

The results of the atmospheric parameters and calculated fundamental parameters are listed in Table 2. This shows that the mass estimated in this work is close to the mass from MSC. Hence, to achieve the best consistency between the dynamical mass sum and Al-Wardat's method, we propose a new dynamical parallax for the system of $\pi_{dyn} = 19.14 \pm 0.30$ mas using Equation (9).

3.5. HIP 51255

The triple system FIN 308 consists of the visual binary system (A, B) that was resolved by Tokovinin et al. (2015b) with a period of $P = 32.76$ yr and a component (C) that orbits it with a period of $P = 634.31$ yr. The position angle of this system is $\sim 180°$ different from its astronomical calendar, but quadruple reflection is not allowed by the comprehensive subsystem.

In this work, we used a magnitude difference for the primary system (AB, C) of $\triangle m_V^{Ab,C} = 3.85$ mag and the subsystem (AB) of $\triangle m_V^{Ab} = 0.53$ mag; both values were taken from MSC (Tokovinin 2018c). The results of the atmospheric parameter and calculated fundamental parameter are listed in Table 2.

Figure 7 shows the positions of the system components on the H-R diagram with the evolutionary tracks and age line of 7.08 Gyr. Components A and B left the main sequence to the subgiant phase, while component C is still on the main sequence.

The estimated mass sum using Al-Wardat's method is consistent with the mass sum from MSC. Depending on the estimated mass sum of the subsystem (A, B) from this work and orbital parameters from (Tokovinin 2018c), a new dynamical parallax is calculated (using Equation (9)) as $\pi_{dyn} = 11.02 \pm 0.50$ mas.

3.6. HIP 54611

The nonhierarchical triple system HD 97145 is an almost equilateral triangular configuration consisting of a main
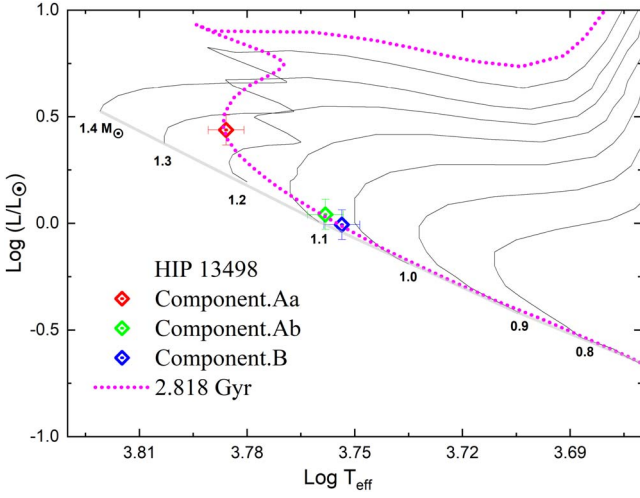
Figure 5. Analysis for HIP 13498. The positions of the components are shown on the H-R diagram with evolutionary tracks and the 2.818 Gyr isochrone with $Z = 0.03$.
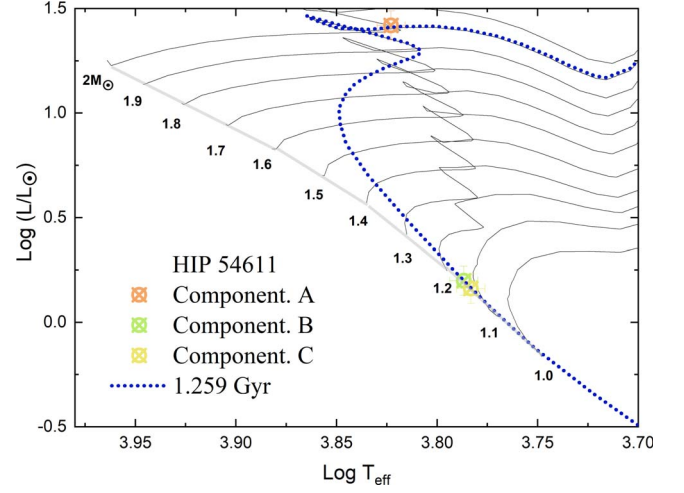

Figure 8. Analysis for HIP 54611. The positions of the components are shown on the H-R diagram with evolutionary tracks and the 1.259 Gyr isochrone with $Z = 0.019$.
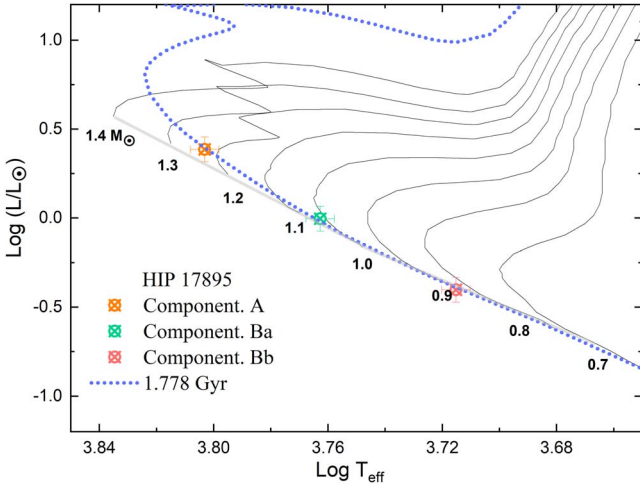

Figure 6. Analysis for HIP 17895. The positions of the components are shown on the H-R diagram with evolutionary tracks and the 1.778 Gyr isochrone with $Z = 0.019$.
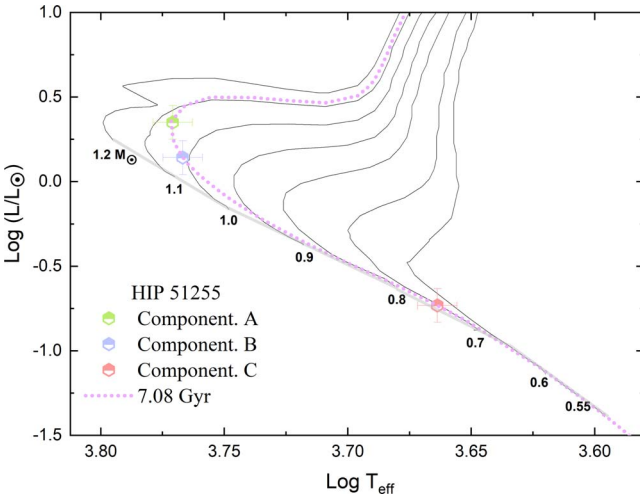
component (A) and subsystem (B, C) with spectral type F5IV/V. According to Tokovinin et al. (2016), all system components are evolved off the main sequence, and component A is located around the 2 Gyr age line. Tokovinin et al. (2016) estimated the masses of the components from the isochrones as $\mathcal{M}_A = 1.6$, $\mathcal{M}_B = 1.0$, and $\mathcal{M}_C = 1.0 \mathcal{M}_\odot$ and also got statistical periods for A and BC of $P = 940$ yr and B and C of $P = 110$ yr.

In this work, we used a magnitude difference for the primary system (A, BC) of $\triangle m_V^{A,BC} = 2.40$ mag and the subsystem (B, C) of $\triangle m_V^{BC} = 0.10$ mag; both values were taken from MSC (Tokovinin 2018c). The results of the atmospheric parameters and calculated fundamental parameters are listed in Table 2(b).

Figure 8 shows the positions of the system components on the H-R diagram with the evolutionary tracks and age line of 1.259 Gyr. Component A has evolved to be subgiant, and components B and C are still located on the main sequence.

The calculated masses and mass sum in this work are listed in Table 2(b). This shows that the mass we estimated is close to the mass sum from MSC.

3.7. HIP 89234

Object HD 165259 is a triple system with comparable separation with an outer orbital period of 400 yr and inner orbital period of 42.1 yr. This system is a triple in WDS (Makarov & Fabricius 2021). The subsystem (Aa, Ab) was first resolved in 2008 at SOAR and named TOK 58. The faint comrade was resolved in Hipparcos at a separation of $2.''32$ and position angle of $259°.6$; it is also present in Gaia DR3 with a separation of $2.''103$ and position angle of $270°.7$. This suggests that the pair is slowly moving counterclockwise on the sky with a long period.

In this work, we used a magnitude difference for the main system (AB) of $\triangle m_V^{Ab} = 3.27$ mag and the subsystem (Aa, Ab) of $\triangle m_V^{AaAb} = 4.17$ mag; both values were taken from MSC (Tokovinin 2018c). The results of the atmospheric parameters and calculated fundamental parameters are listed in Table 2.

Figure 9 shows the positions of the system's components on the H-R diagram, the evolutionary tracks, and the age line of 1.413 Gyr. The massive component (Aa) is evolved off the
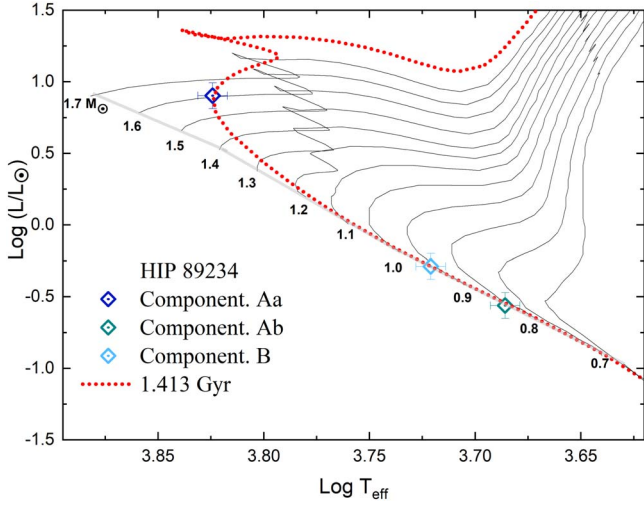

Figure 7. Analysis for HIP 51255. The positions of the components are shown on the H-R diagram with evolutionary tracks and the 7.08 Gyr isochrone with $Z = 0.019$.

Figure 9. Analysis for HIP 89234. The positions of the components are shown on the H-R diagram with evolutionary tracks and the 1.413 Gyr isochrone with $Z = 0.03$.

Figure 10. Analysis for HIP 111805. The positions of the components are shown on the H-R diagram with evolutionary tracks and the 3.548 Gyr isochrone with $Z = 0.008$.

main sequence to the subgiant stage, while components Ab and B are still on the main sequence.

The calculated masses and mass sum in this work are listed in Table 2. This shows that the mass we estimated is almost equal to the dynamical solution using all parallaxes. From the result of the mass, a new dynamical parallax is calculated as $\pi_{\rm dyn} = 23.6029 \pm 0.15$ mas using Equation (9).

3.8. HIP 111805

The triple mineral-poor system HD 214608 consists of a subsystem (Ba, Bb) that was resolved for the first time by Balega et al. (2002); it belongs to the visual pair secondary component HDO 295 (ADS 16138), known since 1887. Horch et al. (2015) derived the masses for the system component as $\mathcal{M}_A = 1.12$, $\mathcal{M}_{Ba} = 0.92$, and $\mathcal{M}_{Bb} = 0.77 \mathcal{M}_\odot$ using standard relations ignoring low metallicity.

Tokovinin & Latham (2017) calculated the orbital elements for the primary system (A, B) and subsystem (Ba, Bb). In addition, they calculated the mass sum of the system as $3.06 \mathcal{M}_\odot$ and a dynamical parallax of $\pi_{\rm dyn} = 24.1$ mas.

In this work, we used a magnitude difference of the primary system (AB) of $\triangle m_V^{\rm Ab} = 0.50$ mag and the subsystem (Ba, Bb) of $\triangle m_V^{\rm AaAb} = 2.04$ mag; both values were taken from MSC (Tokovinin 2018c). The results of the atmospheric parameters and calculated fundamental parameters are listed in Table 2.

Figure 10 shows the positions of the system's components on the H-R diagram, the evolutionary tracks, and the age line of 3.548 Gyr. It shows that components A and Ba have started evolving off the main sequence, while component B is still on the main sequence.

The calculated masses and mass sum in this work are listed in Table 2. From these masses and orbital parameters, a new dynamical parallax is calculated as $\pi_{\rm dyn} = 24.898 \pm 0.25$ mas using Equation (9).

4. Analysis of Quadruple Systems

The quadruple systems analyzed in this study have two different hierarchical structures. The first is a two-tier hierarchy (two close binaries orbiting each other), also called a 2+2
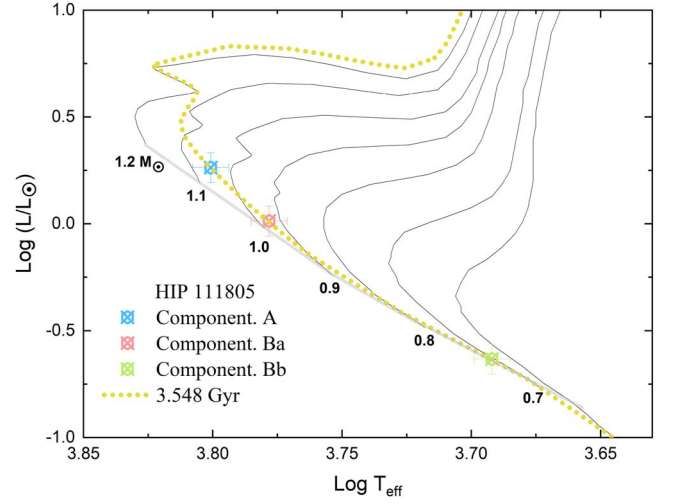
quadruple, such as HIP 12548, HIP 22607, HIP 25240, HIP 28614, and HIP 41171. The second is a three-tier hierarchy, where a close binary has a tertiary component, and this triple is orbited by another distant star, such as HIP 5588, HIP 19915, HIP 51966, and HIP 78977. These systems are called a 3+1 or "planetary" hierarchy.

Figure 11 shows the best fit for the composed synthetic SED for nine quadruple systems (black lines). The dotted and dashed lines are the synthetic SEDs for the individual stars. Moreover, the Johnson magnitude system from Table 1 can be converted to flux density F_λ in units of erg cm^{-2} s^{-1} Å^{-1}, where the effective central wavelength for the blue filter is 4353 nm, and that for the visual filter is 5477 nm. The blue points are the measured blue magnitude by the Johnson filter, and the green points are the measured visual magnitude by the Johnson filter (from Hipparcos ESA 1997).

Table 3(a) lists the 17 parameters (magnitudes and color indices) obtained in the present work for the nine quadruple systems. The systems HIP 12548, HIP 22607, HIP 25240, HIP 28614, and HIP 41171 are 2+2 hierarchy quadruple systems. The systems HIP 5588, HIP 19915, HIP 51966, and HIP 78977 are 3+1 hierarchy quadruple systems.

Table 3(b) lists the atmospheric and fundamental parameters of the nine quadruple systems as obtained in the present work. The columns give the Hipparcos identifier, effective temperatures $T_{\rm eff}$, radii R, logarithm of gravity acceleration $\log g$, luminosities L, bolometric magnitudes $M_{\rm bol}$, absolute visual magnitudes M_V, individual masses $\mathcal{M}$, spectral types Sp, and ages. Masses and ages are estimated from the positions of the subcomponents on the H-R diagram, evolutionary tracks, and isochrones, which are taken from Girardi et al. (2000a).

4.1. HIP 5588

The quadruple system HD 7119 is known as an Am/δ metallic-line star. Through RV observations of the system using the CORAVEL instrument at the Observatory of Haute-Provence, a double-lined spectroscopic binary (Aa, Ab) of the variable value of V_0 was found. The difference in this parameter in terms of orbital motion was explained by the existence of an invisible third component with a much more extended period (Carquillat et al. 2002). Through observation
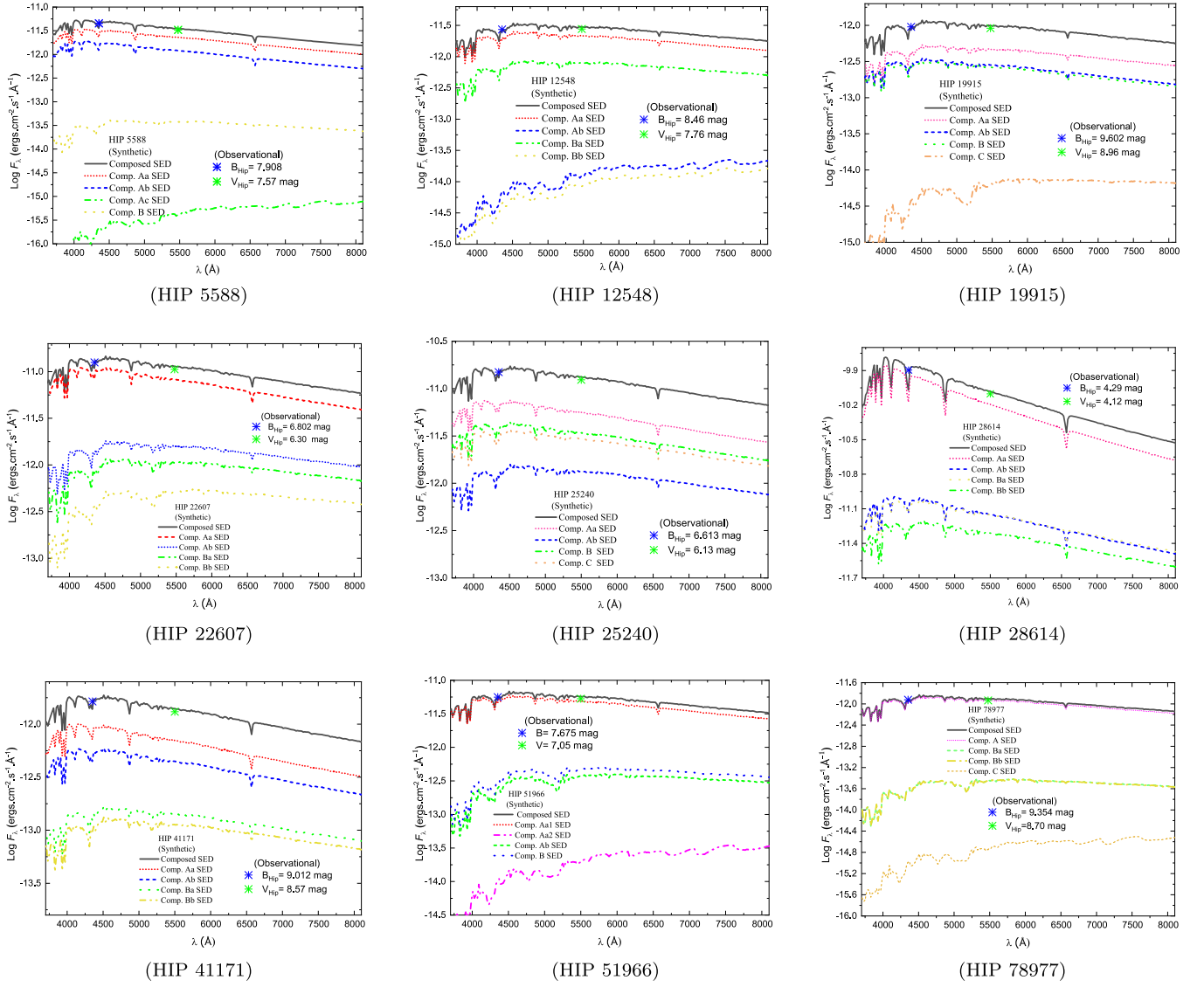
Figure 11. Synthetic SED diagrams for the nine quadruple systems. The four dotted and dashed lines are the SEDs from the individual stars, while the black line is the sum of the individual SEDs (composed). The blue points are the calculated flux density using the measured blue Johnson magnitude, and the green points are the calculated flux density using the measured visual Johnson magnitude (from Hipparcos ESA 1997).

during 1992–1998, the orbital elements of both short and long orbits were derived, as the orbits are well defined. The orbital cycle for a short period is $P = 6.761$ days, and that for the extended period is $P = 1687$ days. The third component can be a cool dwarf with a mass of at least $\mathcal{M} = 0.5\ \mathcal{M}_\odot$; it lies at $a = 0''016$ from the primary subsystem. Therefore, this component cannot be the visual companion that Couteau discovered with a separation of $3''35$. So, the system HIP 5588 is a quadruple system consisting of a triple subsystem (Aa, Ab, and Ac) and a visual fourth single component (B; see Figure 1).

To analyze the system, we used a magnitude difference of the main system (AB) of $\triangle m_V^{Ab} = 4.94$ mag and the internal subsystem (Aa, Ab) of $\triangle m_V^{Ab} = 0.70$ mag. Both values were taken from MSC (Tokovinin 2018c). But the subsystem (Aa, Ab) is a single-lined spectroscopic binary, which means that there is no direct method to measure the magnitude difference. Instead, we used the analytical equation given by (Docobo & Andrade 2013), where we used the individual masses given by the MSC (Tokovinin 2018c), which gives $\triangle m_V = 9.77$ mag. Despite that, there is no metallicity measurement for the

system; we found that all components lie on the same age line of 1 Gyr and metallicity $Z = 0.019$. The calculated and estimated atmospheric and fundamental parameters are listed in Table 2.

Figure 12 shows the positions of the system components on the H-R diagram, the evolutionary tracks, and the age line of 1 Gyr. The figure shows that components Aa and Ab belong to the subgiant phase, while components Ac and B are still in the main-sequence phase. The analysis shows that all components lie on the age line of 1 Gyr. The estimated mass sums using Al-Wardat's method and different parallax measurements are given in Table 4.

4.2. HIP 12548

Object HD 17215 is a hierarchy 2+2 quadruple system belonging to the solar neighborhood and consisting of two inner single-lined spectroscopic binary pairs (Aa, Ab and Ba, Bb) with periods of $P = 1851.9 \pm 18.4$ and $108.18 \pm 18.40.10$ days, respectively (Tokovinin 2022). The outer visual orbit AB

Table 3
(a) 17 Parameters of the Nine Quadruple Systems

Filter	Johnson							Strömgren							Tycho		
	U	B	V	R	$U-B$	$B-V$	$V-R$	u	v	b	y	$u-v$	$u-b$	$b-y$	B_T	V_T	B_T-V_T
HIP 5588																	
Obs.	...	...	7.908	7.57	...	...	0.338	...	...	...	...	...	...	0.195	7.974	7.591	0.383
Comp.	7.92	7.91	7.57	7.38	0.01	0.337	0.19	9.14	8.15	7.76	7.55	0.99	0.39	0.22	7.99	7.62	0.37
Aa	8.38	8.38	8.03	7.84	0.01	0.34	0.20	9.61	8.62	8.23	8.01	0.98	0.39	0.22	8.46	8.08	0.38
Ab	9.05	9.03	8.73	8.56	0.02	0.30	.17	10.29	9.27	8.90	8.71	1.03	0.36	0.19	9.11	8.77	0.33
Ac	19.93	18.80	17.34	16.42	1.12	1.47	0.91	21.41	19.53	18.34	17.34	1.88	1.19	1.02	19.12	17.54	1.57
B	13.66	13.31	12.52	12.09	0.36	0.79	0.42	14.81	13.73	12.94	12.48	1.08	0.79	0.46	13.51	12.60	0.91
HIP 12548																	
Obs.	...	8.46	7.76	...	...	0.700	...	...	...	...	...	...	...	0.438	8.658	7.857	0.801
Comp.	8.69	8.46	7.76	7.39	0.22	0.700	0.38	9.83	8.84	8.15	7.73	0.99	0.69	0.42	8.64	7.84	0.80
Aa	8.96	8.78	8.11	7.76	0.18	0.67	0.36	10.11	9.13	8.48	8.08	0.97	0.65	0.40	8.95	8.19	0.76
Ab	16.22	15.08	13.65	12.77	1.15	1.43	0.88	17.69	15.80	14.59	13.63	1.89	1.21	0.96	15.38	13.85	1.53
Ba	10.36	9.99	9.21	8.79	0.36	0.79	0.42	11.50	10.42	9.64	9.17	1.08	0.79	0.46	10.21	9.29	0.91
Bb	16.64	15.52	14.05	13.134	1.12	1.47	0.91	18.13	16.24	15.06	14.04	1.88	1.19	1.02	15.83	14.26	1.57
HIP 19915																	
Obs.	...	9.602	8.96	...	...	0.642	...	...	...	...	...	...	...	0.399	9.602	9.049	0.553
Comp.	9.75	9.59	8.96	8.61	0.15	0.641	0.35	10.89	9.94	9.32	8.93	0.95	0.63	0.39	9.76	9.03	0.73
Aa	10.69	10.47	9.78	9.41	0.21	0.69	0.37	11.83	10.84	10.16	9.75	0.99	0.68	0.42	10.65	9.86	0.79
Ab	10.96	10.89	10.31	10.00	0.08	0.57	0.31	12.12	11.20	10.64	10.29	0.92	0.56	0.35	11.02	10.38	0.64
B	7.02	6.99	6.70	6.53	0.03	0.30	0.17	8.26	7.23	6.87	6.67	1.03	0.36	0.19	7.07	6.74	0.33
C	16.78	15.69	14.48	13.75	1.09	1.21	0.73	18.15	16.41	15.12	14.40	1.74	1.28	0.72	15.99	14.63	1.36
HIP 22607																	
Obs.	6.85	6.802	6.30	5.84	0.06	0.502	...	...	...	...	...	...	...	0.324	6.857	6.314	0.543
Comp.	6.85	6.80	6.30	6.01	0.05	0.502	0.29	8.04	7.09	6.59	6.27	0.94	0.51	0.32	6.92	6.36	0.56
Aa	7.08	7.07	6.65	6.40	0.01	0.42	0.24	8.27	7.34	6.89	6.62	0.93	0.45	0.27	7.17	6.69	0.47
Ab	9.39	9.16	8.45	8.07	0.24	0.71	0.38	10.54	9.54	8.84	8.42	1.01	0.69	0.42	9.34	8.53	0.81
Ba	10.04	9.68	8.90	8.48	0.36	0.79	0.42	11.12	10.11	9.32	8.86	1.08	0.79	0.46	9.89	8.98	0.91
Bb	11.28	10.63	9.70	9.17	0.65	0.94	0.52	12.47	11.17	10.18	9.64	1.30	0.98	0.54	10.89	9.79	1.09
HIP 25240																	
Obs.	...	6.613	6.13	...	...	0.483	...	...	...	...	...	...	...	0.318	6.695	6.143	0.552
Comp.	6.63	6.61	6.13	5.86	0.02	0.483	0.27	7.81	6.89	6.41	6.10	0.91	0.49	0.31	6.72	6.19	0.54
Aa	7.50	7.49	7.06	6.81	0.01	0.43	0.25	8.69	7.77	7.31	7.04	0.93	0.45	0.28	7.59	7.12	0.48
Ab	9.44	9.28	8.63	8.28	0.16	0.65	0.35	10.59	9.63	8.99	8.60	0.96	0.63	0.39	9.44	8.71	0.73
B	8.12	8.09	7.60	7.33	0.02	0.49	0.28	9.29	8.39	7.89	7.58	0.91	0.50	0.31	8.22	7.66	0.55
C	8.32	8.29	7.77	7.48	0.04	0.52	0.29	9.49	8.58	8.06	7.74	0.91	0.52	0.32	8.41	7.83	0.58
HIP 28614																	
Obs.	4.40	4.29	4.12	3.92	0.08	0.170	...	...	...	...	...	...	...	0.093	4.347	4.150	0.197
Comp.	4.36	4.29	4.12	4.04	0.074	0.170	0.08	5.68	4.48	4.20	4.10	1.19	0.28	0.09	4.35	4.15	0.20
Aa	4.58	4.50	4.40	4.36	0.07	0.10	0.04	5.91	4.67	4.44	4.38	1.24	0.24	0.05	4.55	4.42	0.13
Ab	7.18	7.18	6.80	6.59	0.001	0.37	0.21	8.39	7.43	7.02	6.78	0.96	0.41	0.24	7.26	6.85	0.41

Abu-Alrob, Hussein, & Al-Wardat

Table 3
(Continued)

Filter	Johnson							Strömgren							Tycho		
	U	B	V	R	$U-B$	$B-V$	$V-R$	u	v	b	y	$u-v$	$u-b$	$b-y$	B_T	V_T	B_T-V_T
Ba	7.24	7.24	6.81	6.57	0.005	0.42	0.24	8.44	7.50	7.06	6.79	0.93	0.45	0.27	7.33	6.87	0.47
Bb	7.73	7.71	7.21	6.93	0.02	0.49	0.28	8.90	7.99	7.49	7.18	0.91	0.50	0.31	7.82	7.27	0.55
HIP 41171																	
Obs.	⋯	9.012	8.57	⋯	⋯	0.442	⋯	⋯	⋯	⋯	⋯	⋯	⋯	0.285	9.139	8.685	0.454
Comp.	9.03	9.01	8.57	8.32	0.02	0.442	0.25	10.23	9.29	8.83	8.54	0.94	0.46	0.28	9.11	8.62	0.49
Aa	9.81	9.81	9.42	9.20	0.001	0.39	0.22	11.02	10.07	9.65	9.39	0.95	0.42	0.25	9.90	9.47	0.43
Ab	10.08	10.08	9.66	9.42	0.004	0.42	0.24	11.28	10.35	9.90	9.63	0.93	0.44	0.27	10.17	9.71	0.46
Ba	11.69	11.57	10.96	10.63	0.12	0.61	0.33	12.84	11.90	11.31	10.93	0.94	0.59	0.37	11.72	11.03	0.69
Bb	12.38	12.16	11.46	11.09	0.22	0.69	0.37	13.52	2.53	11.85	11.43	0.99	0.68	0.42	12.33	11.54	0.80
HIP 51966																	
Obs.	⋯	7.675	7.05	⋯	⋯	0.625	⋯	⋯	⋯	⋯	⋯	⋯	⋯	0.392	7.782	7.137	0.645
Comp.	7.80	7.67	7.05	6.70	0.13	0.625	0.35	8.96	8.01	7.40	7.02	0.95	0.61	0.38	7.82	7.12	0.71
Aa1	7.87	7.79	7.22	6.90	0.08	0.57	0.31	9.03	8.11	7.54	7.19	0.92	0.56	0.35	7.93	7.28	0.64
Aa2	15.75	14.61	13.18	12.30	1.14	1.43	0.89	17.23	15.34	14.13	13.16	1.90	1.21	0.97	14.92	13.38	1.54
Ab	11.88	11.08	10.07	9.48	0.79	1.01	0.58	13.11	11.67	10.59	10.00	1.43	1.086	0.59	11.36	10.18	1.17
B	11.52	10.79	9.81	9.26	0.73	0.98	0.55	12.73	11.36	10.32	9.75	1.37	1.04	0.56	11.06	9.92	1.14
HIP 78977																	
Obs.	⋯	9.354	8.70	8.07	0.654	⋯	⋯	⋯	⋯	⋯	⋯	⋯	⋯	⋯	9.516	8.788	0.728
Comp.	9.52	9.35	8.70	8.35	0.16	0.654	0.35	10.67	9.70	9.07	8.67	0.96	0.64	0.39	9.52	8.77	0.74
A	9.57	9.42	8.78	8.43	0.15	0.64	0.35	10.72	9.76	9.14	8.75	0.95	0.63	0.39	9.58	8.85	0.73
Ba	14.31	13.58	12.606	12.05	0.73	0.98	0.55	15.52	14.15	13.11	12.55	1.37	1.04	0.56	13.85	12.72	1.14
Ab	14.28	13.57	12.606	12.06	0.71	0.97	0.55	15.48	14.13	13.10	12.55	1.35	1.02	0.56	13.84	12.71	1.12
C	18.30	17.15	15.74	14.88	1.16	1.41	0.86	19.78	17.88	16.64	15.71	1.90	1.23	0.93	17.45	15.94	1.51

(b) Atmospheric and Fundamental Parameters of the Nine Quadruple Systems

Comp.	$T_{\rm eff}$, K	R, $R_\odot$	$\log g$, cm s^{-2}	L, $L_\odot$	$M_{\rm bol}$, mag	M_V, mag	$\mathcal{M}$, $\mathcal{M}_\odot$	Sp	Age,[a] Gyr
HIP 5588									
Aa	7100	3.8	3.58	32.95	0.96	0.97	2.06	F1/IV	1
Ab	7350	2.56	3.88	17.17	1.66	1.66	1.85	A9/IV	
Ac	3940	0.435	4.85	0.04	8.22	9.33	0.5	K8/V	
B	5490	0.886	4.46	0.64	5.23	5.40	0.84	G8/V	
HIP 12548									
Aa	5860	1.34	4.23	1.90	4.05	4.15	1.12	G1/V	5.012
Ab	4010	0.497	4.79	0.06	7.85	8.85	0.56	K7/V	
Ba	5490	0.96	4.45	0.75	5.06	5.22	0.97	G8/V	
Bb	3940	0.466	4.81	0.05	8.07	9.18	0.52	K8/V	
HIP 19915									

Table 3
(Continued)

				(b) Atmospheric and Fundamental Parameters of the Nine Quadruple Systems					
Aa	5775	2	3.86	3.99	3.25	3.36	1.07	G2/IV	6.31
Ab	6170	1.33	4.19	2.30	3.84	3.91	1.02	F8/IV	
B	6170	1.284	4.22	2.15	3.92	3.99	1.01	F8/IV	
C	4460	0.555	4.72	0.11	7.15	7.82	0.6	K5/V	
				HIP 22607					
Aa	6720	1.45	4.24	3.85	3.29	3.32	1.37	F3/V	1.122
Ab	5720	0.925	4.50	0.82	4.96	5.08	1	G3/V	
Ba	5490	0.841	4.54	0.58	5.35	5.52	0.92	G8/V	
Bb	5050	0.75	4.59	0.33	5.96	6.25	0.81	K2/V	
				HIP 25240					
Aa	6680	1.73	4.13	5.35	2.93	2.97	1.49	F4/V	1.259
Ab	5920	1.11	4.39	1.36	4.42	4.51	1.13	G0/V	
B	6440	1.464	4.23	3.31	3.45	3.50	1.34	F5.5/V	
C	6355	1.40	4.26	2.87	3.61	3.66	1.31	F6/V	
				HIP 28614					
Aa	8770	2.846	3.89	43.02	0.67	0.77	2.32	A2/IV	0.5012
Ab	6810	1.531	4.21	4.53	3.11	3.13	1.40	F2/V	
Ba	6810	1.523	4.21	4.48	3.12	3.14	1.40	F2/V	
Bb	6550	1.38	4.26	3.15	3.51	3.55	1.30	F5/V	
				HIP 41171					
Aa	6880	1.65	4.15	5.47	2.90	2.91	1.44	F1/V	1.259
Ab	6740	1.545	4.20	4.61	3.09	3.11	1.39	F2/V	
Ba	6040	1.09	4.40	1.42	4.37	4.45	1.11	F9/V	
Bb	5760	0.975	4.45	0.94	4.82	4.93	1.00	G2/V	
				HIP 51966					
Aa1	6160	1.33	4.18	2.29	3.85	3.92	1.00	F8/IV	7.08
Aa2	4070	0.413	4.87	0.04	8.19	9.19	0.47	K7/V	
Ab	4940	0.665	4.64	0.24	6.32	6.67	0.72	K2.5/V	
B	5050	0.695	4.62	0.28	6.12	6.41	0.74	K2/V	
				HIP 78977					
A	5940	2.58	3.75	7.44	2.57	2.66	1.40	G0/IV	3.612
Ba	4970	0.741	4.61	0.30	6.05	6.40	0.83	K2.5/V	
Bb	4940	0.757	4.59	0.31	6.03	6.38	0.82	K2.5/V	
C	4050	0.48	4.81	0.06	7.89	8.89	0.55	K7/V	

Note.

[a] The isochrones are functions of the metallicity.
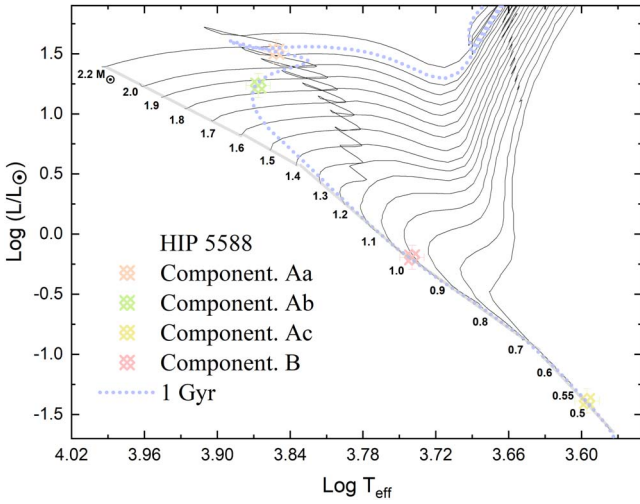
Figure 12. Analysis for HIP 5588. The positions of the components are shown on the H-R diagram with evolutionary tracks and the 1 Gyr isochrone with $Z = 0.019$.

1923 has been known since 1931 with a period of $P = 106.3$ yr. (Nordström et al. 2004) assumed that there is a spectroscopic subsystem, and they determined its mass ratio by $q = 0.26$, but their results were not used because they did not include the RV measurements. Tokovinin (2022) derived the orbital elements of the visual orbits (A, B) and of the spectroscopic orbits of subsystems Aa, Ab and Ba, Bb. He also estimated the masses of the components. Tokovinin (2022) also used the estimate along with the orbital solution of the main system to calculate the dynamical parallax as $\pi_{orb} = 18.5$ mas. In this work, we used a magnitude difference of the primary system (AB) of $\triangle m_V^{Ab} = 1.11$ mag, but the subsystems (Aa, Ab and Ba, Bb) are single-lined spectroscopic binaries, which means that there is no direct method to measure the magnitude difference. So, to calculate the magnitude difference of the subsystems, we used Equation (2) and the individual masses proposed by Tokovinin (2022). This gives magnitude differences for subsystems Aa, Ab and Ba, Bb of $\triangle m_V^{AaAb} = 5.54$ and $\triangle m_V^{BaBb} = 4.84$ mag. The results of the atmospheric parameters and calculated fundamental parameters are listed in Table 2. Figure 13 shows the positions of the system's components on the H-R diagram with the evolutionary tracks and age line of 5.012 Gyr. It shows that component Aa started to evolve off the main sequence, while the other components are still in the main-sequence phase. The estimated mass sum in this work is listed in Table 2. Depending on the estimated mass sum, a new dynamical parallax is calculated (using Equation (9)) as $\pi_{dyn} = 17.23 \pm 0.75$ mas.

4.3. HIP 19915

The triple system HD 26872 consists of a double-lined inner subsystem (Aa, Ab) with a period of 7.3 days, which lies at a large inclination with the primary system AB. The system AB, which is known as YSC 128, consists of a narrow 32 mas interferometric pair with an approximate period of ∼6 yr (Sperauskas et al. 2019). It has no solution of its orbit yet. In the Geneva–Copenhagen spectroscopic survey, the system was found to be of poor metallicity, with a metal abundance of $[Fe/H] = -2.01$ (Holmberg et al. 2009), which gives a strange value of Z of 0.00019. It was found to be $[Fe/H] = -0.36$ according to Gaia Collaboration et al. (2016), which gives a

low-metallicity system of $Z = 0.008$. A double-lined spectroscopic binary with a mass ratio $q = 0.904 \pm 0.019$ was also observed, and it is not the same spectroscopic system, YSC 128, previously detected. It is a comprehensive system with a faint component at a separation of $0.''5$; it is an AB pair with a C component (Horch et al. 2019). So the whole system is a quadruple system instead of a triple one.

In this work, we used a magnitude difference of the primary system (AB) with C of $\triangle m_V^{Ab} = 5.55$ mag and the subsystem (AB) of $\triangle m_V^{Ab} = 1.10$ mag. Both values were taken from MSC (Tokovinin 2018c). For the inner subsystem (Aa, Ab), the magnitude difference according to the MSC is equal to $\triangle m_V^{AaAb} = 0$ mag, but the masses are different, not equal, so we did not use this value; instead, we calculated another value of $\triangle m_V^{AaAb} = 0.53$ mag using the analytical equation (Docobo & Andrade 2013), and the individual masses are given in the MSC. The results of the atmospheric parameters and calculated fundamental parameters are listed in Table 2. Figure 14 shows the positions of the system's components on the H-R diagram, the evolutionary tracks, and the age line of 6.31 Gyr of the figure. It shows that components Aa, Ab, and B are already evolved off the main sequence to the subgiant stage, while component C is still on the main sequence. The estimated masses and mass sum in this work are listed in Table 2.

4.4. HIP 22607

The hierarchical quadruple system HD 30869 belongs to the e Hyades cluster. The outer visual pair (AB) known as BU 552 has been known since 1877. Its orbit has been well defined through observations covering 1.5 revolutions with a period of 95 yr. Components A and B are double-lined spectroscopic binaries with periods of 143.6 and 496.7 days, respectively (Tomkin et al. 2007).

Tomkin et al. (2007) suggested a spectral type and an individual mass of component Aa of F5 and $\mathcal{M}_{Aa} = 1.4\ \mathcal{M}_\odot$, component Ab of G8 and $\mathcal{M}_{Ab} = 0.9\ \mathcal{M}_\odot$, component Ba of K1/2 and $\mathcal{M}_{Ba} = 0.8\ \mathcal{M}_\odot$, and component Bb of K6 and $\mathcal{M}_{Bb} = 0.68\ \mathcal{M}_\odot$; these values give a mass sum of $\Sigma\mathcal{M} = 3.78\ \mathcal{M}_\odot$.

In this work, we used a magnitude difference of the primary system (AB) of $\triangle m_V^{Ab} = 2.01$ mag, the subsystem Aa, Ab of $\triangle m_V^{AaAb} = 1.8$ mag, and the subsystem Ba, Bb of $\triangle m_V^{BaBb} = 0.8$ mag. All values were taken from MSC (Tokovinin 2018c). The results of the atmospheric parameters and calculated fundamental parameters are listed in Table 2.

Figure 15 shows the positions of the system's components on the H-R diagram, the evolutionary tracks, and the age line of 1.122 Gyr. It shows that component Aa is starting to evolve off the main sequence, while components Ab, Ba, and Bb are still on the main sequence.

The calculated masses and mass sum in this work are listed in Table 2(b), which shows that the mass we estimated is closer to the MSC and farther from the dynamical mass using the Hipparcos 2 parallax. That shows that there is a problem with the Hipparcos 2 parallax of this system. From the result of the mass, a new dynamical parallax of $\pi_{dyn} = 21.88 \pm 0.9$ mas using Equation (9) can be suggested.

4.5. HIP 25240

The bright hierarchy 2+2 quadruple system HR 1782 (HD 35317) consists of two inner pairs; the first is a double-lined

Table 4
Comparison between the Dynamical Mass Sums Calculated Depending on Orbital Elements (Once Available), MSC Mass Sums, and Those Estimated Using Al-Wardat's Method in This Work

HIP	System	P yr	a arcsec	Source	$\Sigma\mathcal{M}^H_{dyn}$ $\mathcal{M}_\odot$	$\Sigma\mathcal{M}^{G2}_{dyn}$ $\mathcal{M}_\odot$	$\Sigma\mathcal{M}^{G3}_{dyn}$ $\mathcal{M}_\odot$	$\mathcal{M}^1_{MSC}$ $\mathcal{M}_\odot$	$\mathcal{M}^2_{MSC}$ $\mathcal{M}_\odot$	$\Sigma\mathcal{M}_{MSC}$ $\mathcal{M}_\odot$	$\Sigma\mathcal{M}_{TW}$ $\mathcal{M}_\odot$	π_{dyn} mas
(1)	(2)	(4)	(4)	(5)	(6)	(7)	(8)	(9)	(10)	(11)	(12)	(13)
4239	AB	…	…	…	…	…	…	3.05	0.86	3.91	4.01	
	Aa, Ab	10.8640	0.0719	[1]	3.38	3.70	3.365	1.62	1.43	3.05	3.09	10.064
5588	AB	…	…	…	…	…	…	4.70	0.84	5.54	5.33	
	Aab, Ac	…	…	…	…	…	…	4.2	0.5	4.7	4.41	
	Aa, Ab	…	…	…	…	…	…	2.2	2	4.2	3.91	
11072	AB	26.54	0.5344	[2]	2.30	2.53	2.738	1.33	1.20	2.53	2.45	44.55
	Ba, Bb	…	…	…	…	…	…	0.6	0.6	1.2	1.2	
12548	AB	106.3	0.568	[3]	2.52	4.08	…	1.39	1.2	2.59	3.17	17.23
	Aa, Ab	5.07	0.0117	[3]	0.01	0.02	…	1.07	0.32	1.39	1.68	
	Ba, Bb	…	…	…	…	…	…	0.89	0.31	1.19	1.49	
13498	AB	51.46	0.2960	[4]	3.48	31.309	5.70	2.07	0.93	3	3.36	14.25
	Aa, Ab	…	…	…	…	…	…	1.11	0.96	1.89	2.11	
17895	AB	51.10	0.3834	[5]	2.86	…	…	1.14	1.78	2.92	3.08	19.14
	Ba, Bb	…	…	…	…	…	…	0.96	0.82	1.78	1.86	
19915	AB, C	…	…	…	…	…	…	3.36	0.64	4	3.7	
	A, B	…	…	…	…	…	…	2.25	1.11	3.36	3.1	
	Aa, Ab	…	…	…	…	…	…	1.19	1.06	2.25	2.09	
22607	AB	97.71	0.7430	[6]	2.90	3.69	3.699	2.30	1.67	3.97	4.10	21.88
	Aa, Ab	…	…	…	…	…	…	1.34	0.96	2.3	2.37	
	Ba, Bb	…	…	…	…	…	…	0.91	0.76	1.67	1.73	
25240	A, BC	1200	3.716	[7]	6.16	5.02	4.763	2.68	2.33	5.01	5.27	18.91
	Aa, Ab	…	…	…	…	…	…	1.50	1.18	2.68	2.62	
	B, C	47.03	0.3366	[8]	2.98	2.43	2.304	1.19	1.14	2.33	2.65	
28614	AB	18.6410	0.273	[9]	6.36	12.72	…	3.03	2.75	5.78	6.42	20.93
	Aa, Ab	0.0122	0.002	[9]	5.76	11.55	…	2.38	0.65	3.03	3.72	
	Ba, Bb	0.0131	0.002	[9]	4.50	10.2	…	1.39	1.36	2.75	2.70	
41171	AB	…	…	…	…	…	…	2.70	2.09	4.79	4.94	
	Aa, Ab	…	…	…	…	…	…	1.47	1.23	2.70	2.83	
	Ba, Bb	…	…	…	…	…	…	1.09	1.00	2.09	2.11	
51255	A, BC	…	…	…	…	…	…	2.12	0.71	2.83	2.80	
	A, B	32.76	0.1440	[12]	1.97	3.32	2.03	1.11	1.01	2.12	2.09	11.02
51966	AB	205.00	1.334	[10]	3.58	2.53	3.092	2.12	0.72	2.84	2.93	26.81
	Aa, Ab	8.8464	0.15	[11]	2.72	1.93	2.361	1.40	0.72	2.12	2.19	
	Aa1, Ab2	0.473067	0.0184	[11]	1.76	1.25	1.524	1.20	0.30	1.40	1.47	
54611	A, BC	…	…	…	…	…	…	1.92	2.0	3.92	4.16	
	B, C	…	…	…	…	…	…	1.01	0.99	2.0	2.26	
78977	AB, C	…	…	…	…	…	…	3.36	0.50	3.86	3.60	
	A, B	…	…	…	…	…	…	1.44	1.92	3.36	3.05	
	Ba, Bb	…	…	…	…	…	…	0.98	0.94	1.92	1.65	
89234	AB	400	1.923	[13]	3.33	3.31	3.341	2.19	0.82	3.01	3.30	23.6029
	Aa, Ab	42.10	0.363	[13]	2	1.99	2.029	0.73	0.82	2.19	2.40	
111805	AB	30.1270	0.3361	[14]	2.33	…	…	1.14	1.88	3.02	2.71	24.898
	Ba, Bb	1.5012	0.0385		1.41	…	…	1.03	0.85	1.74	1.66	

Note. Source of orbital elements: [1] Tokovinin et al. (2019). [2] Fekel et al. (2018). [3] Tokovinin (2022). [4] Tokovinin (2016). [5] Gorynya & Tokovinin (2018). [6] Tokovinin et al. (2019). [7] Tokovinin (2018b). [8] Tokovinin (2018b). [9] Muterspaugh et al. (2008). [10] Tokovinin et al. (2015a). [11] Tokovinin et al. (2015a). [12] Tokovinin et al. (2015b). [13] Tokovinin (2018d). [14] Tokovinin & Latham (2017).

spectroscopic binary (Aa, Ab) with periods of 22.58 days (Tokovinin 1997), and the second is a visual pair with periods of 47 yr (Tokovinin 2018b). They revolve around each other on a wide, poorly constrained outer orbit with a period of 1000 yr. Tokovinin (2018b) modified the orbital solution of the outer orbit (AB with C), where gave new values for the
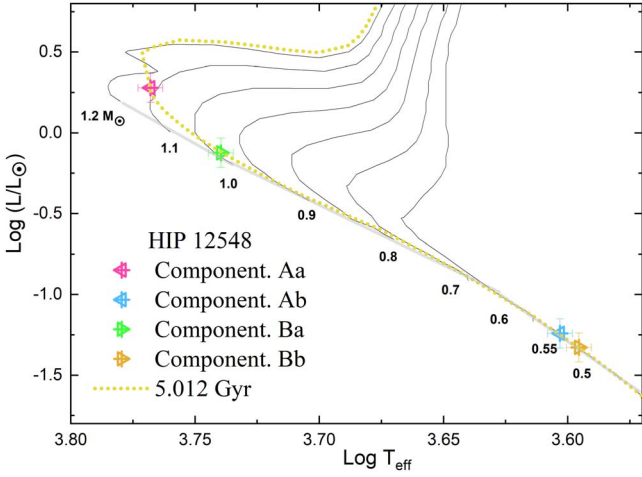
Figure 13. Analysis for HIP 12548. The positions of the components are shown on the H-R diagram with evolutionary tracks and the 5.012 Gyr isochrone with $Z = 0.03$.
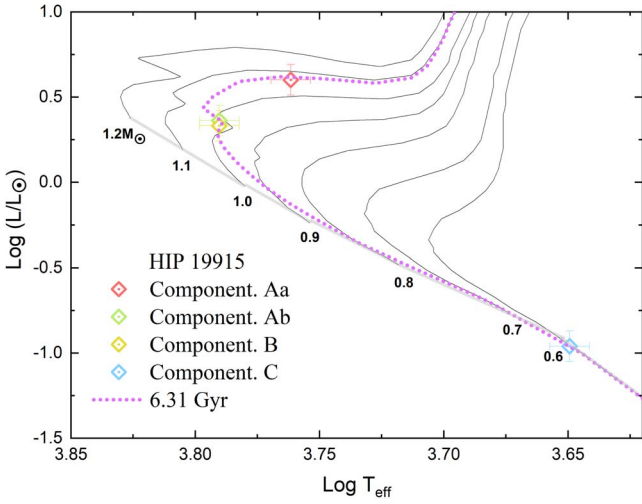

Figure 14. Analysis for HIP 19915. The positions of the components are shown on the H-R diagram with evolutionary tracks and the 6.31 Gyr isochrone with $Z = 0.008$.
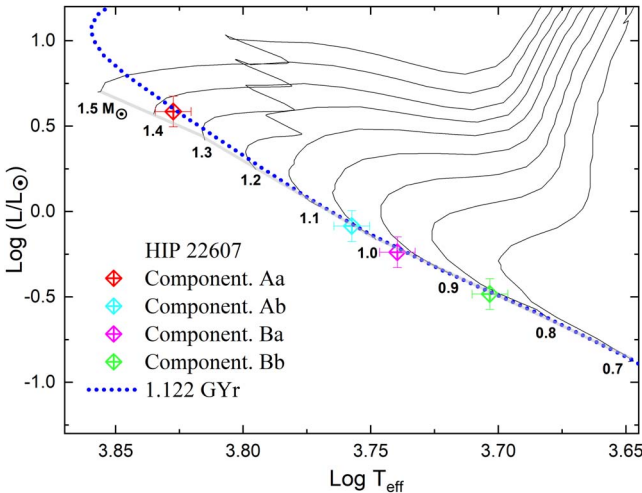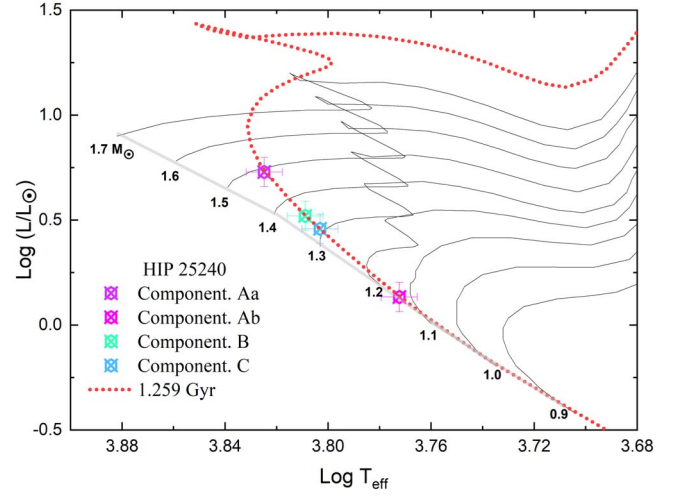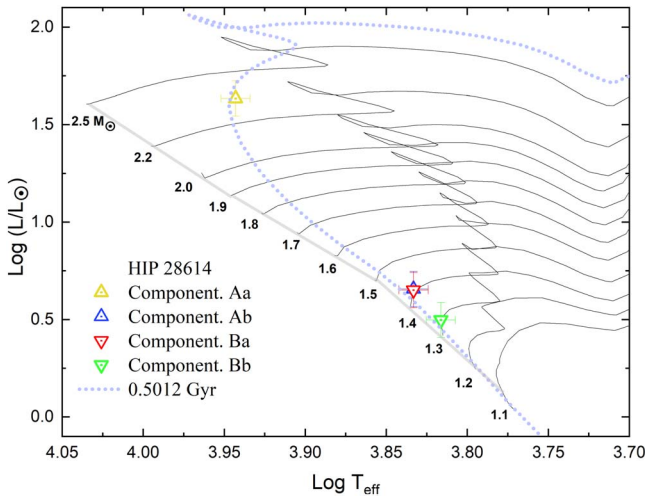

Figure 15. Analysis for HIP 22607. The positions of the components are shown on the H-R diagram with evolutionary tracks and the 1.122 Gyr isochrone with $Z = 0.019$.

Figure 16. Analysis for HIP 25240. The positions of the components are shown on the H-R diagram with evolutionary tracks and the 1.259 Gyr isochrone with $Z = 0.03$.

period and eccentricity were given as ($P = 1200$ yr, $e = 0.2$), which gave a reasonable outer mass sum. The measures published of the $3''$ A, B pair in 2015 September, which was made in SOAR distorted by aliasing. (Tokovinin 2018b) corrected and confirmed through the new measurements in 2017 September.

Tokovinin (2018b) derived the orbital elements of the primary system (A, BC) and visual pair (B, C). The derived masses from Tokovinin (2018b) of B and C are 1.07 and 1.55 $\mathcal{M}_\odot$, respectively; the mass sum of their mass is equal to $\Sigma \mathcal{M}_{B,C} = 2.62 \ \mathcal{M}_\odot$, and the mass sum of the outer orbit is $5.40 \mathcal{M}_\odot$ using the Gaia DR1 parallax ($\pi_G = 18.75 \pm 0.47$).

In this work, we used a magnitude difference of the primary system (A, BC) of $\triangle m_V^{A,BC} = 0.1$ mag, the subsystem Aa, Ab of $\triangle m_V^{AaAb} = 1.57$ mag, and the subsystem B, C of $\triangle m_V^{BC} = 0.17$ mag; all values were taken from MSC (Tokovinin 2018c). The results of the atmospheric parameters and calculated fundamental parameters are listed in Table 2.

Figure 16 shows the positions of the system's components on the H-R diagram with the evolutionary tracks and age line of 1.259 Gyr. Components Aa, B, and C have started to evolve off the main sequence, while component Ab is still on the main sequence.

The calculated masses and mass sum in this work are listed in Table 2. The mass we estimated is closer to the dynamical solution using the Gaia DR1 parallax, and the total mass of the visual pair (B, C) is almost equal to the total mass, which Tokovinin (2018b) derived. From the result of the mass, a new dynamical parallax of $\pi_{\rm dyn} = 18.91 \pm 0.9$ mas using Equation (9) can be suggested.

4.6. HIP 28614

The hierarchical bright quadruple system μ Orionis (61 Ori, HR 2124, and HD 40932) can be seen with the naked eye. It is located north of Betelgeuse. This system has been extensively studied by RV and teqneique (speckle, interferometry, Occultation, and Hipparcos). Component Aa was discovered by (Frost 1906) in a short-period (4.5 days) single-lined spectroscopic binary, but component Ab is of low mass and has not been directly detected. Aitken (1914) discovered that the system had a more distant component (B) that forms a

Figure 17. Analysis for HIP 28614. The positions of the components are shown on the H-R diagram with evolutionary tracks and the 0.5012 Gyr isochrone with $Z = 0.019$.

subarcsecond visual binary. Long after, it was discovered by (Fekel 1980) that B was a short-period (4.78 days) double-lined spectroscopic binary; since then, the system has been considered a quadruple system.

Using stellar evolution models predicting isochrones for elements of this system, Muterspaugh et al. (2008) estimated the age of component Aa to be in the range [0.1–0.316] Gyr, and this age is incompatible with the age of components Ba and Bb, which are located at an age of 1 Gyr.

Docobo & Andrade (2006) suggested a spectral type, an apparent magnitude, and an individual mass for component Aa of A1V, $m_V^{Aa} = 4.4 \pm 0.2$ mag, and $\mathcal{M}_{Aa} = 2.7 \mathcal{M}_\odot$; component Ab of F5V, $m_V^{Ab} = 6.8 \pm 0.3$ mag, and $\mathcal{M}_{Ab} = 1.2 \mathcal{M}_\odot$; component Ba of F5V, $m_V^{Ba} = 3.2 \pm 0.1$ mag, and $\mathcal{M}_{Ba} = 1.2 \mathcal{M}_\odot$; and component Bb of F7V, $m_V^{Bb} = 7.2 \pm 0.1$ mag, and $\mathcal{M}_{Bb} = 1.1 \mathcal{M}_\odot$. These values give a mass sum of $\Sigma \mathcal{M} = 6.2 \mathcal{M}_\odot$.

In this work, we used a magnitude difference for the main system (AB) of $\triangle m_V^{Ab} = 1.95$ mag from (Tokovinin 2018c), the subsystem Aa, Ab of $\triangle m_V^{AaAb} = 2.4$, and the subsystem Ba, Bb of $\triangle m_V^{BaBb} = 0.40$ mag; all values were taken from (Docobo & Andrade 2006). The results of the atmospheric parameters and calculated fundamental parameters are listed in Table 2(b).

Figure 17 shows the positions of the system's components on the H-R diagram and evolutionary tracks of 0.5012 Gyr. The most massive component (Aa) is already evolved off the main sequence to the subgiant stage, while components Ab, Ba, and Bb have started to evolve from the main sequence. The calculated masses and mass sum in this study are listed in Table 2. This shows that the mass we estimated is very close to the dynamical solution using the Hipparcos 2 parallax and far from the solution from the Gaia DR2 parallax. From the result of the mass, a new dynamical parallax of $\pi_{dyn} = 20.93$ using Equation (9) can be suggested. This dynamical parallax is close to the value of the reduced Hipparcos parallax ($\pi_{(H)} = 21.05 \pm 0.68$ mas) and far from the value given by Gaia DR2 ($\pi_{G2} = 16.6954 \pm 1.4291$ mas). That shows the relative reliability of the Hipparcos measurements compared to Gaia DR2, as noted by Al-Wardat et al. (2021a).

4.7. HIP 41171

The outer visual pair (AB; RST 4396) was discovered in 1940 by R. A. Rossiter with a separation of $1''$ and an estimated period of ~1 kyr, but this pair has not been solved yet. This has a very long outer period, while the inner periods are concise, so there is no significant $\triangle \mu$ for discovering astronomical acceleration. This system consists of two internal systems; the first component (A) is a double-lined spectroscopic binary separated into two components (Aa, Ab) with an orbital period of 25.4160 days discovered by (Nordström et al. 2004). The second component (B) discovered through more monitoring is also a double-lined spectroscopic binary (Ba, Bb) with an orbital period of 963 days, separated into two components. The age of the system is expected to be relatively young due to the possible existence of a weak lithium line in the spectra of Aa and Ab and the measurable rotation of these stars. Tokovinin (2019b) estimated the effective temperature, spectral type, absolute magnitude, and individual mass of components Aa and Ab as $T_{eff}^{Aa} = 6500$ K, F5V, $M_V^{Aa} = 9.41$ mag, and $\mathcal{M}_{Aa} = 1.28 \mathcal{M}_\odot$ and $T_{eff}^{Ab} = 6400$ K, F6V, $M_V^{Ab} = 9.65$ mag, and $\mathcal{M}_{Aa} = 1.23 \mathcal{M}_\odot$, respectively, with a measured mass ratio of $q = 0.97$. He estimated the effective temperature and absolute magnitude of B as $T_{eff}^B = 5900$ K and $M_V^B = 10.93$ mag, but these estimates are preliminary.

In this work, we used a magnitude difference for the main system (A, B) of $\triangle m_V^{Ab} = 1.65$ mag, the subsystem Aa, Ab of $\triangle m_V^{AaAb} = 0.24$ mag, and the subsystem Ba, Bb of $\triangle m_V^{BaBb} = 0.50$ mag; all values were taken from MSC (Tokovinin 2018c). The results of the atmospheric parameters and calculated fundamental parameters are listed in Table 2(b).

Figure 18 shows the positions of the system's components on the H-R diagram, the evolutionary tracks, and the age line of 1.259 Gyr. It is shown that components Aa and Ab have started evolving off the main sequence, while components Ba and Bb are still located on the main sequence.

The calculated masses and mass sum in this work are listed in Table 2(b), which shows that the mass we estimated in this work is close to that of MSC.

4.8. HIP 51966

The hierarchical quadruple system HD 91962 has a three-tiered planetary structure revolving around the most massive central star, Aa1. The spectral type of this system is G1V (Wright et al. 2003). The outer system (main system) A and B were discovered in 1903 (Aitken 1904); its orbit was calculated for the first time by (Popovic & GM 1978) with a period of 283 yr. It was recalculated by (Tokovinin et al. 2014) for 200 yr. The subsystem Aa, Ab was discovered by (Metchev & Hillenbrand 2009) with adaptive optics in 2003.354 at $0.''142$, $56.°2$. The spectroscopic system (Aa, Ab) was independently solved by (Tokovinin et al. 2010) in 2009 through SOAR interferometry. In 2012.18, it was seen at the same position as 2003.354, thus completing an entire revolution in 3233 ± 20 days (8.85 yr). The inner spectroscopic system (Aa1, Aa2) was discovered for 170.3 days.

Tokovinin et al. (2015a) calculated the orbital elements for the primary system (AB), the subsystem (Aa, Ab), and the internal subsystem (Aa1, Aa2). Hence, they calculated the mass sum of the system as $2.75 \mathcal{M}_\odot$, distributed as $\mathcal{M}_{Aa1} = 1.10$, $\mathcal{M}_{Aa2} = 0.30$, $\mathcal{M}_{Ab} = 0.64$, and $\mathcal{M}_B = 0.64 \mathcal{M}_\odot$. From the orbital solution of the primary system and mass sum,
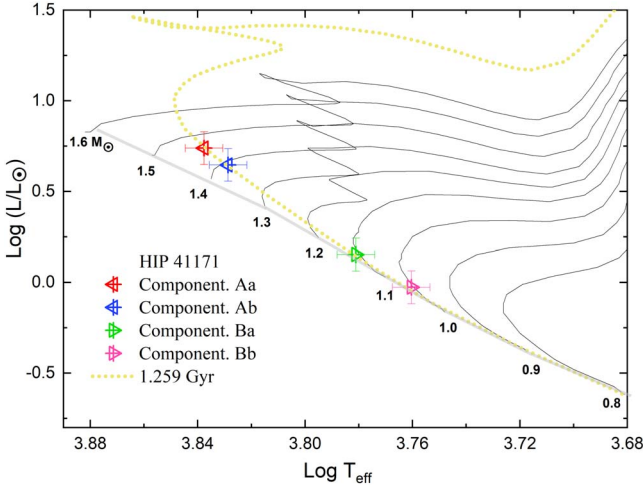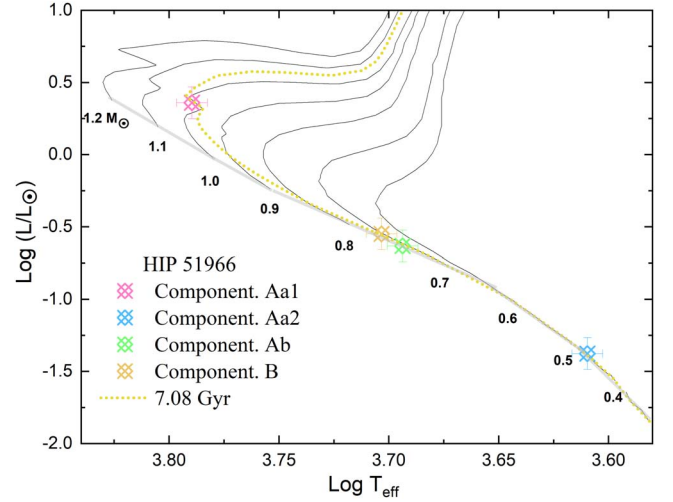
Figure 18. Analysis for HIP 41171. The positions of the components are shown on the H-R diagram with evolutionary tracks and the 1.259 Gyr isochrone with $Z = 0.019$.

Tokovinin et al. (2015a) calculated the dynamical parallax as $\pi_{\mathrm{orb}} = 27.4$ mas.

In this work, we used a magnitude difference for the primary system (AB) of $\triangle m_V^{\mathrm{Ab}} = 2.67 \pm 0.10$ mag and the subsystem (Aa, Ab) of $\triangle m_V^{AaAb} = 2.86 \pm 0.10$ mag; both values were taken from (Tokovinin et al. 2015a). The inner subsystem (Aa1, Aa2) is a single-lined spectroscopic binary. There is no direct method to measure the magnitude difference, so we calculate the magnitude difference using Equation (2); the magnitude difference between Aa1 and Aa2 is $\triangle m_V = 5.96$. The results of the atmospheric parameters and calculated fundamental parameters are listed in Table 2.

Figure 19 shows the positions of the system's components on the H-R diagram, the evolutionary tracks, and the age line of 3.548 Gyr at metallicity $Z = 0.008$ i. It shows that component Aa1 evolved off the main sequence to the subgiant stage, while components Aa2, Ab, and B are still on the main sequence.

The calculated masses and mass sum in this work are listed in Table 2(b). This shows that the mass we estimated is close to the dynamical mass sum using the Gaia DR3 parallax and farther from the Gaia DR2 parallax. From the result of the mass, a new dynamical parallax of $\pi_{\mathrm{dyn}} = 26.81 \pm 0.5$ mas using Equation (9) can be suggested.

4.9. HIP 78977

The triply eclipsing system HD 144548 consists of a detached eclipsing system (Ba, Bb) with a period of $P = 1.63$ days orbiting around a primary star (A) with a period of $P = 33.945$ days forming a compact hierarchical with a comprehensive component (C) with a period of $P = 6453.4$ yr, as given in MSC. The triple system is the first triply eclipsing system that can measure the RVs of all of their components Alonso et al. (2015); this triple system is rare.

Alonso et al. (2015) extracted the mass and radius of the components of the triple system: component A, $\mathcal{M}_A = 1.44\mathcal{M}_\odot$ and $R_A = 2.41\ R_\odot$; component Ba, $\mathcal{M}_{Ba} = 0.984\mathcal{M}_\odot$ and $R_{Ba} = 1.319\ R_\odot$; and component Bb, $\mathcal{M}_{Bb} = 0.984\mathcal{M}_\odot$ and $R_{Bb} = 1.319\ R_\odot$. It has been observed that the radii obtained from the components are about 65% larger than the main-sequence star for component A and about 40% larger than the main-sequence star for components Ba and

Figure 19. Analysis for HIP 51966. The positions of the components are shown on the H-R diagram with evolutionary tracks and the 7.08 Gyr isochrone with $Z = 0.008$.
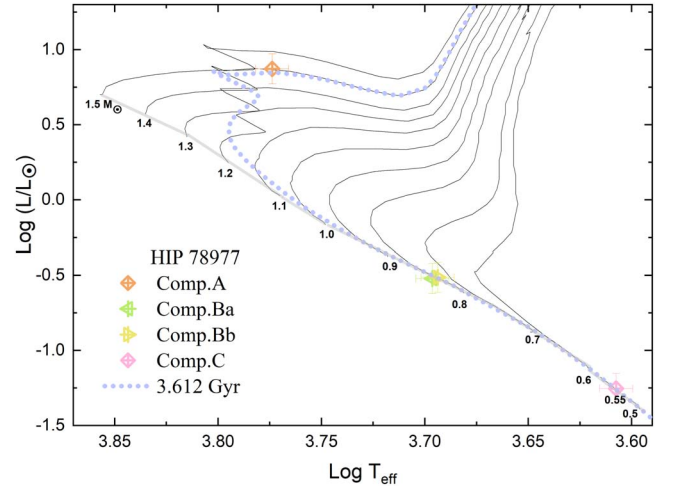

Figure 20. Analysis for HIP 78977. The positions of the components are shown on the H-R diagram with evolutionary tracks and the 3.612 Gyr isochrone with $Z = 0.019$.

Bb. Most models suggested the age of this star to be around 8–11 Myr. However, David et al. (2015) noted the dispersion of the true age of this star, and it was observed that the most massive component (A) is several Myr younger than the eclipsing system B.

David et al. (2019) studied the atmospheric parameters of the components of the triple system HIP 78977. They determined that component A has a spectral type of F7.5 with an effective temperature of $T_{\mathrm{eff}}^A = 6210 \pm 80$ K] while components Ba and Bb are both K5 with effective temperatures of $T_{\mathrm{eff}} = 4210 \pm 200$ K].

In this work, we used a magnitude difference for the primary system (AB, C) of $\triangle m_V^{\mathrm{Ab},C} = 7.05$ mag, the system AB of $\triangle m_V^{\mathrm{Ab}} = 3.07$ mag, and the system Ba, Bb of $\triangle m_V^{BaBb} = 0$; all values were taken from MSC (Tokovinin 2018c). The results of the atmospheric parameters and calculated fundamental parameters are listed in Table 2(b).

Figure 20 shows the positions of the system components on the H-R diagram with the evolutionary tracks and age line of 3.612 Gyr at metallicity $z = 0.019$. Component A left the main sequence for the subgiant phase, while the others were still on
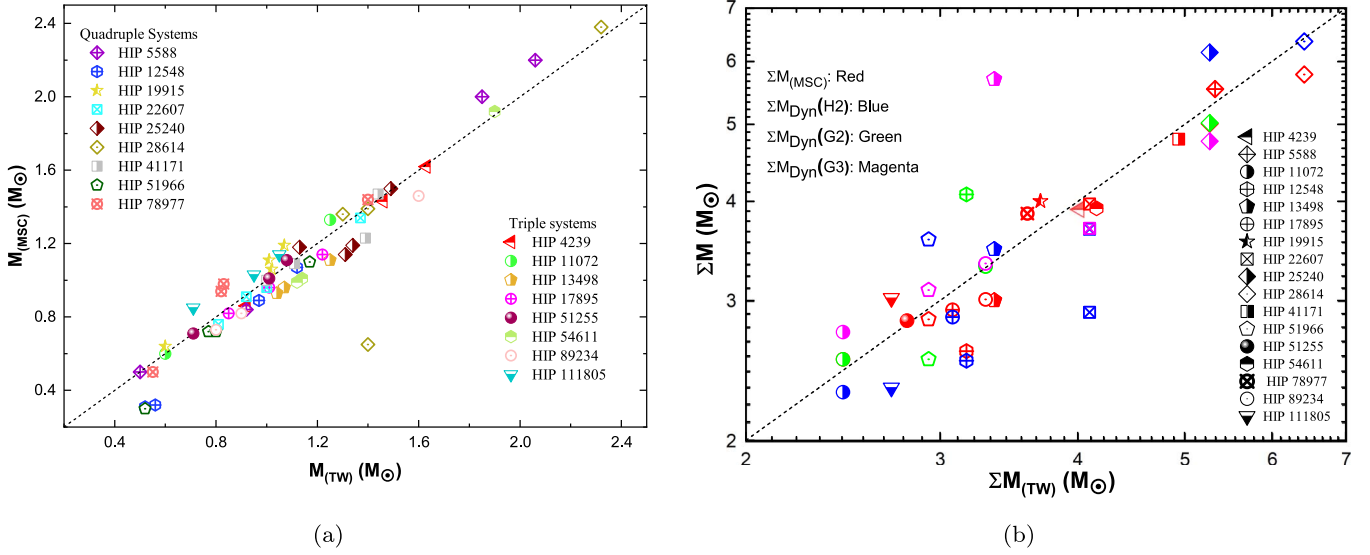
Figure 21. Mass comparisons. (a) Comparison between individual component masses from MSC and those estimated using Al-Wardat's method. (b) Comparison between the dynamical mass sums calculated depending on orbital elements, MSC mass, and those estimated using Al-Wardat's method. Based on the Hipparcos 2 parallax (blue), Gaia DR2 parallax (green), Gaia DR3 (magenta), and MSC (red). The dotted line represents $y = x$.
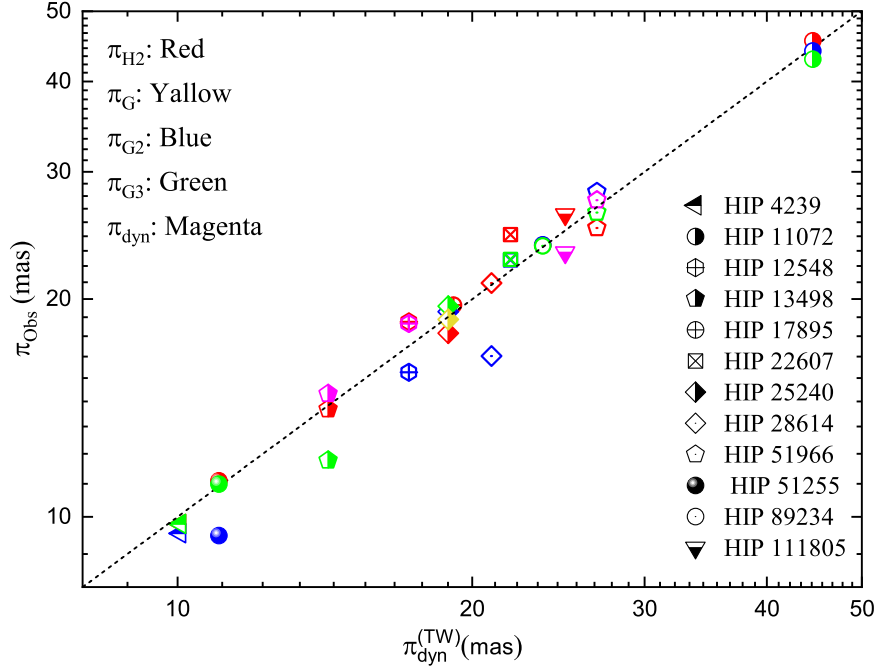

Figure 22. Comparison between the dynamical parallax calculated in this work and the Hipparcos 2 (red), Gaia DR2 (blue), Gaia DR3 (green), dynamical (magenta), and Gaia DR1 (yellow) parallaxes (only for HIP 25240). The line represents $y = x$.

the main sequence. This work shows that the components are located at the same age, 3.612 Gyr. The estimated age does not match with the assumed age because they assumed that the massive component (A) had not evolved, and our analysis shows that this component evolved to the subgiant stage. The estimated mass sum using Al-Wardat's method is somewhat close to the mass sum from MSC.

5. Masses and Parallaxes

Table 4 gives a comparison between the dynamical mass sums calculated using Kepler's third law depending on the orbital solutions (once available) and using the three parallax measurements (columns (6)–(8)), the masses given by the MSC

as the mass of the primary component(s) (column (9)), the mass of the secondary component(s) (column (10)), the total mass (column (11)), the mass sum estimated in this work as $\Sigma \mathcal{M}$ (column (12)) depending on different parallax measurements, and the dynamical mass (column (13)). Five of these systems are without any orbital solution for the main or subsystem; these are HIP 5588, HIP 19915, HIP 41171, HIP 54611, and HIP 78977.

So, to get a better picture of the masses, we plotted the correlations in Figure 21.

Figure 21(a) shows a comparison between the individual masses estimated in this work using Al-Wardat's method and those given by MSC (see Table 4). Figure 21(b) shows a
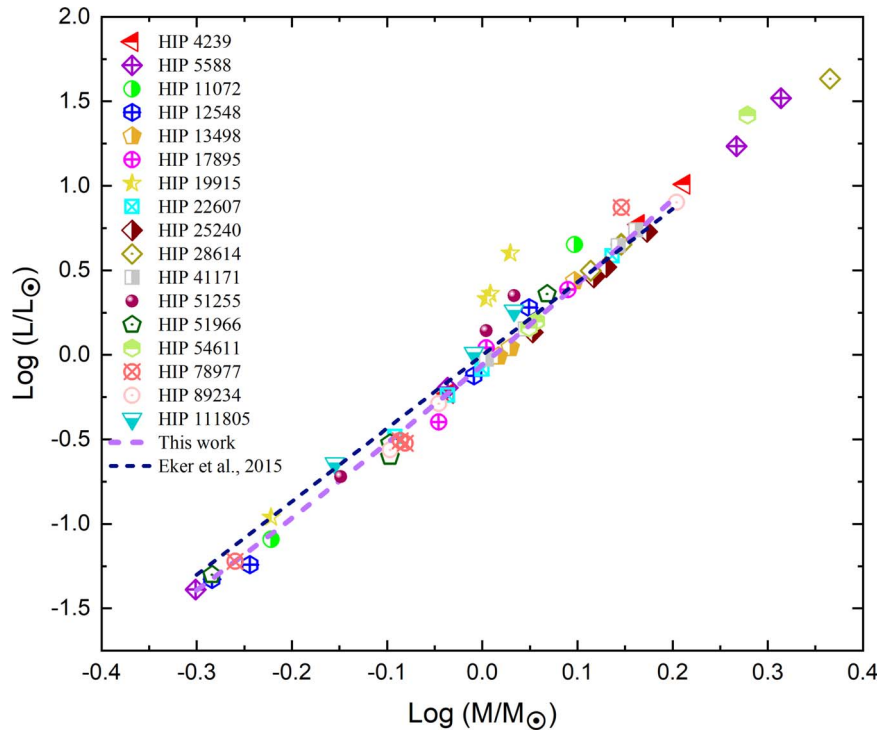
Figure 23. Best quadratic curve fitting as the MLR for the whole sample compared to the linear MLRs of Eker et al. (2015).

comparison between the mass sum of individual components estimated in this work and those given by MSC (red) and the dynamical mass sum recalculated using the Hipparcos (blue), Gaia DR2 (green), and Gaia DR3 (magenta) parallaxes (see Table 4).

The comparison shows an excellent consistency between Al-Wardat's individual masses and the masses given in MSC for most components. Although there are four outliers (component Ab of HIP 28614, component Ab and Bb of HIP 12548, and component Aa2 of HIP 51966), it is because the method used in that source gives the estimation of the minimum mass of the secondary component, since the system is a single-lined spectroscopic binary.

So, once we have an excellent orbital solution for the system (either visual or spectroscopic orbits for any level of the hierarchical composition), we can calculate a new dynamical parallax for the system using the following equation:

$$3\log(\pi_{\mathrm{dyn}}) = 3\log(h) - \log(\Sigma M), \qquad (9)$$

where $\log(h) = \log(a) - \frac{3}{2}\log(P)$. The results of these calculations are listed in column (13) of Table 4.

Figure 22 shows a comparison between the calculated dynamical parallax using Equation (9) in this work using our estimated masses (Table 4, column (13)) and those measured by Hipparcos and Gaia (Table 1, columns (6)–(8)). A detailed discussion of each system is given.

5.1. Mass–Luminosity Relation

There are different works on mass–luminosity relations (MLRs; Griffiths et al. 1988; Duquennoy et al. 1991; Eker et al. 2015 and Wang & Zhong 2018). All of these relations are about main-sequence single stars. So we used our estimated masses and luminosities of the individual components, which

are being given for the first time, to revisit the MLRs and improve the accuracy of the coefficient.

The sample contains 60 stars, including eight triple systems (24 stars) and nine quadruple systems (36 stars), where 16 components of the sample were excluded (14 subgiant stars). Figure 23 shows the estimated MLRs for the 46 main-sequence components. The figure also shows a comparison between our quadratic fit and that given by Eker et al. (2015). The following equation represents the quadratic fit and its coefficients of our MLR:

$$\log\frac{L}{L_\odot} = 0.90\left(\log\frac{\mathcal{M}}{\mathcal{M}_\odot}\right)^2 + 4.71\left(\log\frac{\mathcal{M}}{\mathcal{M}_\odot}\right) - 0.06, \qquad 0.50 \leqslant \mathcal{M} \leqslant 1.60. \qquad (10)$$

As shown, our fit is close to the Eker et al. (2015) fit with some variance for low mass; this is because of the difference in metallicity for some systems.

6. Conclusions

We present the analysis of 17 multiple stellar systems consisting of eight triple systems and nine quadruple systems. Our results of 17 parameters are summarized in Table 2 for the eight triple systems and Table 3 for the nine quadruple systems. The results concerning the atmospheric and fundamental parameters of the systems are given in Tables 2 (triple systems) and 3 (quadruple systems). The calculated masses and dynamical parallax are given in Table 4.

We emphasize that the configurations and magnitude differences of the selected systems were taken from the MSC due to Tokovinin (2018a). These parameters, along with the measurements of the composed visual magnitudes of the systems and the entire color indices from different sources. enable us to analyze these systems using Al-Wardat's method of analyzing the BMSSs.

Depending on the results of the analysis, we can conclude the following.

1. We used the observational Fe/H values along with our results to plot the individual components of the systems on the H-R diagram with evolutionary tracks and isochrones (Girardi et al. 2000a). We used metallicity [$Z = 0.008$, $Y = 0.25$] for analyzing three systems, [$Z = 0.019$, $Y = 0.273$] for analyzing 10 systems, and [$Z = 0.03$, $Y = 0.30$] for analyzing four systems.

2. The positions of the components on the H-R diagram and evolutionary tracks show that 10 of the 60 components are subgiant stars; these are HIP 5588 Aa, HIP 11072 A, HIP 19915 Aa, HIP 19915 Ab, HIP 19915 B, HIP 51255 A, HIP 51255 B, 51966 Aa1, HIP 54611 A, and HIP 78977 A. The rest of the components are main-sequence stars.

3. Using the main-sequence stars, a quadratic fit with new coefficients for the MLR is presented as given in Equation (10).

4. The dynamical parallaxes according to our evaluation show that Gaia DR3 parallax measurements improved well in comparison with Gaia DR2.

5. There are two systems (HIP 13498 and HIP 28614) with an apparent discrepancy in their trigonometric parallax measurements between Gaia and Hipparcos. For the system HIP 13498, Hipparcos 2 gave 14.09 ± 0.73 mas, Gaia DR3 gave 11.9770 ± 0.3677 mas, and Gaia DR2 gave 6.7724 ± 1.1456 mas, while our analysis gives a dynamical value of 14.25 ± 0.60 mas. For the system HIP 28615, Hipparcos 2 gave 21.05 ± 0.68 mas, Gaia DR2 gave 16.6854 ± 1.4291 mas, and the Gaia DR3 parallax measurement is outstanding. Our analysis gives a dynamical parallax of 19.14 ± 0.30 mas for HIP 13498 and 20.93 ± 0.80 mas for HIP 28641. That means that the measurements of Hipparcos 2 are the closest to our dynamical ones, and this agrees with the conclusions of Al-Wardat et al. (2021a) that the Gaia DR2 release has a problem with the parallax measurements of some binary and multiple systems compared with Hipparcos measurements.

ORCID iDs

Enas M. Abu-Alrob ● https://orcid.org/0000-0001-7718-9209
Abdallah M. Hussein ● https://orcid.org/0000-0002-0738-4305
Mashhoor A. Al-Wardat ● https://orcid.org/0000-0002-1422-211X

References

Aitken, R. G. 1904, LicOB, 2, 139
Aitken, R. G. 1914, LicOB, 8, 93
Alonso, R., Deeg, H., Hoyer, S., et al. 2015, A&A, 584, L8
Al-Tawalbeh, Y. M., Hussein, A. M., Taani, A. A., et al. 2021, AstBu, 76, 71
Al-Wardat, M. 2009, AN, 330, 385
Al-Wardat, M. 2012, PASA, 29, 523
Al-Wardat, M., Balega, Y. Y., Leushin, V., et al. 2014a, AstBu, 69, 58
Al-Wardat, M., Balega, Y. Y., Leushin, V., et al. 2014b, AstBu, 69, 198
Al-Wardat, M. A., Abu-Alrob, E., Hussein, A. M., et al. 2021b, RAA, 21, 161
Al-Wardat, M. A., Hussein, A. M., & Abu-Alrob, E. M. 2022, in The Multifaceted Universe: Theory and Observations (Trieste: Sissa), 10
Al-Wardat, M. A. 2002, Bull. Special Astrophys. Obs., 53, 51
Al-Wardat, M. A., Hussein, A. M., & Abu-Alrob, E. M. 2022, AJ, 163, 182
Al-Wardat, M. A., Hussein, A. M., Al-Naimiy, H. M., & Barstow, M. A. 2021a, PASA, 38, e002
Al-Wardat, M. A. 2012, PASA, 29, 523
Balega, I., Balega, Y. Y., Hofmann, K.-H., et al. 2002, A&A, 385, 87
Balega, Y. Y., & Tikhonov, N. 1977, SvAL, 3, 272
Beers, T. C., Placco, V. M., Carollo, D., et al. 2017, ApJ, 835, 81
Bertelli, G., Bressan, A., Chiosi, C., Fagotto, F., & Nasi, E. 1994, A&AS, 106, 275
Bochanski, J. J., Faherty, J. K., Gagné, J., et al. 2018, AJ, 155, 149
Carquillat, J.-M., Ginestet, N., Prieur, J.-L., & Udry, S. 2002, MNRAS, 336, 1043
Casagrande, L., Schönrich, R., Asplund, M., et al. 2011, A&A, 530, A138
Castelli, F., & Kurucz, R. L. 2003, in IAU Symp. 210, Modeling of Stellar Atmospheres, ed. N. Piskunov, W. W. Weiss, & D. F. Gray (San Francisco, CA: ASP), A20
David, T. J., Hillenbrand, L. A., Cody, A. M., Carpenter, J. M., & Howard, A. W. 2015, ApJ, 816, 21
David, T. J., Hillenbrand, L. A., Gillen, E., et al. 2019, ApJ, 872, 161
Docobo, J., & Andrade, M. 2013, MNRAS, 428, 321
Docobo, J. A., & Andrade, M. 2006, ApJ, 652, 681
Docobo, J. A., & Andrade, M. 2013, MNRAS, 428, 321
Duchêne, G., & Kraus, A. 2013, ARA&A, 51, 269
Duquennoy, A., & Mayor, M. 1991, A&A, 248, 485
Duquennoy, A., Mayor, M., & Halbwachs, J.-L. 1991, A&AS, 88, 281
Eker, Z., Soydugan, F., Soydugan, E., et al. 2015, AJ, 149, 131
ESA 1997, ESA SP-1200, The Hipparcos and Tycho Catalogues (ESA) (Noordwijk: ESA)
Fekel, F. C. 1980, PASP, 92, 785
Fekel, F. C., Willmarth, D. W., Abt, H. A., & Pourbaix, D. 2018, AJ, 156, 117
Frost, E. B. 1906, ApJ, 23, 264
Gaia Collaboration 2018, yCat, I/345
Gaia Collaboration, Brown, A. G. A., Vallenari, A., et al. 2016, A&A, 595, A2
Gaia Collaboration, Smart, R. L., Sarro, L. M., et al. 2021, A&A, 649, A6
Gáspár, A., Rieke, G. H., & Ballering, N. 2016, ApJ, 826, 171
Girardi, L., Bressan, A., Bertelli, G., & Chiosi, C. 2000a, A&AS, 141, 371
Girardi, L., Bressan, A., Bertelli, G., & Chiosi, C. 2000b, yCat, 414, 10371
Gorynya, N., & Tokovinin, A. 2018, MNRAS, 475, 1375
Griffiths, S. C., Hicks, R. B., & Milone, E. F. 1988, JRASC, 82, 1
Güdel, M., Schmitt, J., & Benz, A. 1995, A&A, 302, 775
Hartkopf, W. I., Tokovinin, A., & Mason, B. D. 2012, AJ, 143, 42
Hilditch, R. W. 2001, An Introduction to Close Binary Stars (Cambridge: Cambridge Univ. Press)
Holmberg, J., Nordström, B., & Andersen, J. 2009, A&A, 501, 941
Horch, E. P., Robinson, S. E., Ninkov, Z., et al. 2002, AJ, 124, 2245
Horch, E. P., Tokovinin, A., Weiss, S. A., et al. 2019, AJ, 157, 56
Horch, E. P., Van Altena, W. F., Demarque, P., et al. 2015, AJ, 149, 151
Houk, N. 1978, Ann Arbor, Univ. Michigan
Hussein, A. M., Al-Wardat, M. A., Abushattal, A., et al. 2022, AJ, 163, 182
Kurucz, R.-L. 1993, ATLAS9 Stellar Atmosphere Programs and 2 km/s grid. Kurucz CD-ROM No. 13 (Cambridge, MA: Smithsonian Astrophysical Observatory)
Kurucz, R. L. 1995, ApJ, 452, 102
Labeyrie, A. 1970, A&A, 6, 85
Lafreniere, D., Doyon, R., Marois, C., et al. 2007, ApJ, 670, 1367
Lindegren, L., Bastian, U., Biermann, M., et al. 2021, A&A, 649, A4
Maíz Apellániz, J. 2007, in ASP Conf. Ser. 364, The Future of Photometric, Spectrophotometric and Polarimetric Standardization, ed. C. Sterken (San Francisco, CA: ASP), 227
Makarov, V. V., & Fabricius, C. 2021, AJ, 162, 260
Mardini, M. K., Li, H., Placco, V. M., et al. 2019a, ApJ, 875, 89
Mardini, M. K., Placco, V. M., Taani, A., Li, H., & Zhao, G. 2019b, ApJ, 882, 27
Mardini, M. K., Frebel, A., Chiti, A., et al. 2022a, ApJ, 936, 78
Mardini, M. K, Frebel, A., Ezzeddine, R., et al. 2022b, MNRAS, 517, 3993
Masda, S. G., Al-Wardat, M. A., & Pathan, J. M. 2019, RAA, 19, 105
Masda, S. G., Docobo, J. A., Hussein, A. M., et al. 2019, AstBu, 74, 464
Metchev, S. A., & Hillenbrand, L. A. 2009, ApJS, 181, 62
Moe, M., & Di Stefano, R. 2017, ApJS, 230, 15

Muterspaugh, M. W., Lane, B. F., Fekel, F. C., et al. 2008, AJ, 135, 766
Netopil, M. 2017, MNRAS, 469, 3042
Nielsen, E. L., & Close, L. M. 2010, ApJ, 717, 878
Nordström, B., Mayor, M., Andersen, J., et al. 2004, A&A, 418, 989
Pecaut, M. J., & Mamajek, E. E. 2013, ApJS, 208, 9
Popovic, G., & GM, P. 1978, Bulletin de l'Observatoire Astronomique de Belgrade, 129, 9
Raghavan, D., McAlister, H. A., Henry, T. J., et al. 2010, ApJS, 190, 1
Sperauskas, J., Deveikis, V., & Tokovinin, A. 2019, A&A, 626, A31
Tanineah, D. M., Hussein, A. M., Widyan, H., & Al-Wardat, M. A. 2022, AdSpR, 71, 1080
Tokovinin, A. 1997, A&AS, 121, 71
Tokovinin, A. 2013, AJ, 145, 76
Tokovinin, A. 2016, AJ, 152, 11
Tokovinin, A. 2018a, AJ, 156, 194
Tokovinin, A. 2018b, AJ, 155, 160
Tokovinin, A. 2018c, AJ, 156, 48
Tokovinin, A. 2018d, ApJS, 235, 6
Tokovinin, A. 2019a, AJ, 157, 91
Tokovinin, A. 2019b, AJ, 158, 222
Tokovinin, A. 2021, Univ, 7, 352

Tokovinin, A. 2022, AJ, 163, 161
Tokovinin, A., & Cantarutti, R. 2008, PASP, 120, 170
Tokovinin, A., Everett, M. E., Horch, E. P., Torres, G., & Latham, D. W. 2019, AJ, 158, 167
Tokovinin, A., & Latham, D. W. 2017, ApJ, 838, 54
Tokovinin, A., Latham, D. W., & Mason, B. D. 2015a, AJ, 149, 195
Tokovinin, A., Mason, B. D., & Hartkopf, W. I. 2010, AJ, 139, 743
Tokovinin, A., Mason, B. D., & Hartkopf, W. I. 2014, AJ, 147, 123
Tokovinin, A., Mason, B. D., Hartkopf, W. I., Mendez, R. A., & Horch, E. P. 2015b, AJ, 150, 50
Tokovinin, A., Mason, B. D., Hartkopf, W. I., Mendez, R. A., & Horch, E. P. 2016, AJ, 151, 153
Tokovinin, A., Mason, B. D., Mendez, R. A., et al. 2021, AJ, 162, 41
Tomkin, J., Griffin, R., & Alzner, A. 2007, Obs, 127, 87
Vagnozzi, S. 2019, Atoms, 7, 41
van Leeuwen, F. 2007, A&A, 474, 653
von Steiger, R., & Zurbuchen, T. H. 2016, ApJ, 816, 13
Wang, J., & Zhong, Z. 2018, A&A, 619, L1
Wichmann, R., Schmitt, J., & Hubrig, S. 2003, A&A, 400, 293
Wright, C. O., Egan, M. P., Kraemer, K. E., & Price, S. D. 2003, AJ, 125, 359
Yousef, Z. T., Annuar, A., Hussein, A. M., et al. 2021, RAA, 21, 114